The Journal of Experimental Biology 214, 1473-1487

doi:10.1242/jeb.050062

RESEARCH ARTICLE

Claudin 28b and F-actin are involved in rainbow trout gill pavement cell tight junction remodeling under osmotic stress

Adolf Michael Sandbichler, Margit Egg, Thorsten Schwerte and Bernd Pelster*

Institute of Zoology, and Center for Molecular Biosciences, University of Innsbruck, Technikerstr. 25, 6020 Innsbruck, Austria

*Author for correspondence (bernd.pelster@uibk.ac.at)

Accepted 23 December 2010

SUMMARY

Permeability of rainbow trout gill pavement cells cultured on permeable supports (single seeded inserts) changes upon exposure to freshwater or treatment with cortisol. The molecular components of this change are largely unknown, but tight junctions that regulate the paracellular pathway are prime candidates in this adaptational process. Using differential display polymerase chain reaction we found a set of 17 differentially regulated genes in trout pavement cells that had been exposed to freshwater apically for 24 h. Five genes were related to the cell–cell contact. One of these genes was isolated and identified as encoding claudin 28b, an integral component of the tight junction. Immunohistochemical reactivity to claudin 28b protein was concentrated in a circumferential ring colocalized to the cortical F-actin ring. To study the contribution of this isoform to changes in transepithelial resistance and Phenol Red diffusion under apical hypo- or hyperosmotic exposure we quantified the fluorescence signal of this claudin isoform in immunohistochemical stainings together with the fluorescence of phalloidin-probed F-actin. Upon hypo-osmotic stress claudin 28b fluorescence and epithelial tightness remained stable. Under hyperosmotic stress, the presence of claudin 28b at the junction significantly decreased, and epithelial tightness was severely reduced. Cortical F-actin fluorescence increased upon hypo-osmotic stress, whereas hyperosmotic stress led to a separation of cortical F-actin rings and the number of apical crypt-like pores increased. Addition of cortisol to the basolateral medium attenuated cortical F-actin separation and pore formation during hyperosmotic stress and reduced claudin 28b in junctions except after recovery of cells from exposure to freshwater. Our results showed that short-term salinity stress response in cultured trout gill cells was dependent on a dynamic remodeling of tight junctions, which involves claudin 28b and the supporting F-actin ring.

Key words: *Oncorhynchus mykiss*, rainbow trout, pavement cell, single seeded insert, cortisol, claudin 28b, cortical F-actin, tight junction, osmotic stress.

INTRODUCTION

In contrast to the majority of fish, which are stenohaline, euryhaline fish are not restricted to one habitat but can migrate between freshwater (FW), estuarine and marine environments. The gills especially, as the main osmoregulatory organ in fish, undergo tremendous physiological transformations changing from a salt-uptake organ in FW into a salt-excreting organ in seawater (SW). This ability to tolerate different salinities may have evolved independently in different species (Evans et al., 2005). Therefore the one true blueprint for the cellular function of gills may not exist. Nevertheless, the osmotic challenge to euryhaline fish is uniform. In FW the animal is hyperosmotic and gains water. For compensation it starts to actively absorb ions from the dilute habitat, stops drinking and produces large volumes of urine. In SW the fish loses its body water to the hyperosmotic surrounding. For compensation it drinks water and actively excretes excess ions *via* the gills. As a result, despite the osmotic gradient being reversed, the internal ion balance of euryhaline fish is remarkably stable (Takei and Hirose, 2002).

This stability of plasma osmolarity is in large part dependent on the immediate and long-term regulation of active transcellular ion transport processes at the gill epithelium, a field that has been intensively studied in the last few decades. Furthermore, based on observations made by transmission electron microscopy, adaptation to FW or SW also affects the morphology of the gill epithelium, and hence affects the passive ion permeability, leading to a ‘tight’ or ‘leaky’ phenotype, respectively (Sardet et al., 1979; Ernst et al., 1980; Hwang, 1987).

The FW-adapted phenotype of the gill epithelium features tight apical cell–cell contacts between mitochondria-rich (MR) cells and pavement cells, which extend from 200 to 500 nm (Hwang, 1987), whereas in the SW-adapted phenotype MR cells decrease in size and are associated to an accessory cell with shallow (leaky) apical junctions (Karnaky, 1992; Marshall, 1995). These junctions let lanthanum penetrate, whereas deep (tight) apical junctions between pavement cells and between pavement cells and chloride or accessory cells do not (Sardet et al., 1979).

With the introduction of *in vitro* primary pavement cell cultures on permeable supports (single seeded inserts; SSI), it could be shown that under symmetrical conditions (i.e. with apical and basolateral growth medium), it was not only cultures from FW-adapted animals such as the rainbow trout (*Oncorhynchus mykiss*) that developed epithelia with high transepithelial resistance (TER) (Wood and Pärt, 1997), but also pavement cell cultures from marine sea bass (*Dicentrarchus labrax*) (Avella and Ehrenfeld, 1997).

Combining results from ultrastructure imaging and epithelial physiology of FW- and SW-adapted pavement cells it appeared that tight junctions between pavement cells are also ‘tight’ in SW epithelia despite the leaky nature of SW-adapted gills. However, with the use of SSI cultures it could be shown that, although the cultures consisted exclusively of pavement cells, these epithelia also changed their tightness. For example, when incubated with

synthetic FW, SSI cultures transiently increased TER (Gilmour et al., 1998; Kelly and Wood, 2001a; Kelly and Wood, 2001b; Wood and Pärt, 1997) whereas, to our knowledge, the effect of hyperosmotic saline or SW applied apically to SSI cultures was never addressed.

An increase in epithelial tightness could also be observed when cortisol, the major corticosteroid in osmotic adaptation, was added to the basolateral compartment of SSI cultures from rainbow trout (Kelly and Wood, 2001a) and FW tilapia (*Oreochromis niloticus*) (Kelly and Wood, 2002). The authors interpreted the observation as a permanent reduction of paracellular permeability. In a recent study they showed that cortisol increased occludin deposition in the tight junctions of SSI cultures (Chasiotis et al., 2010) and increased the mRNA expression of specific claudin isoforms in pavement cells of the puffer fish (*Tetraodon nigroviridis*) (Bui et al., 2010). In a previous study we observed that cortisol increased tight junction depth, as well as height of cells in the serosal layer in trout SSI cultures (A.M.S., J. Farkas, W. Salvenmoser and B.P., unpublished observation). Thus, pavement cell epithelia can increase their physiological tightness in FW or when exposed to cortisol. Such adaptations affect the permeability of the paracellular pathway, which therefore depends on a dynamic structure of tight junctions.

Recent studies have addressed components of the tight junction complex, especially the large family of claudin isoforms, for their involvement in paracellular regulation of hydromineral balance in fish (Bagherie-Lachidan et al., 2008; Bagherie-Lachidan et al., 2009; Boutet et al., 2006; Bui et al., 2010; Chasiotis et al., 2010; Kalujnaia et al., 2007; Tipsmark et al., 2008b; Tipsmark et al., 2008c; Tipsmark et al., 2008a). Compared with the 24 isoforms of claudins in humans, fish have considerably increased their repertoire of claudin isoforms. For example, the Japanese puffer fish (*Takifugu rubripes*) has evolved 56 isoforms, which are expressed in an organ-specific fashion and may contribute to ion selectivity and physiological adaptation (Loh et al., 2004). Tipsmark et al. identified at least 26 claudin isoforms in EST databases of Atlantic salmon (*Salmo salar*) (Tipsmark et al., 2008b).

The same group then elegantly showed that gill claudin-3 and claudin-4 immunoreactive proteins were elevated in FW-acclimated flounder (Tipsmark et al., 2008c) and reduced in SW-acclimated tilapia (*Oreochromis mossambicus*) (Tipsmark et al., 2008a). Out of several tested claudin isoforms in Atlantic salmon, mRNAs for claudin 10e and claudins 27a and 30 were inversely regulated in the gill depending on the hypo- or hyperosmotic environment (Tipsmark et al., 2008b). Furthermore, it was also shown that cortisol acts in an isoform-specific fashion on the expression of claudin mRNA in cultured puffer fish epithelia (Bui et al., 2010).

Based on these considerations it was hypothesized that osmotic stress in fish gills would not only modify cell contacts involving MR cells but also cell contacts between pavement cells. Using SSI cultures of trout gill cells and differential display PCR we screened the differentially expressed proteins and identified claudin 28b as a prominent candidate possibly contributing to changes in barrier properties of pavement cells under osmotic stress conditions.

MATERIALS AND METHODS

Experimental animals and SSI gill cell culture

Rainbow trout (*Oncorhynchus mykiss*, Walbaum 1792) that were 2 years old and weighed ~250 g were purchased in a local hatchery and were held in a 1500 l plastic tank with running tap water at 15°C and seasonal light conditions. Fish were fed with trout pellets (Agra Tagger, Graz, Austria) once a day *ad libitum* and were free of diseases and injuries.

The SSI culture protocol followed previously published procedures (Wood and Pärt, 1997) with minor modifications. For each cell culture preparation one fish was killed with a sharp blow to the head and subsequent sectioning of the spinal cord. Gill arches were collected in Ca^{2+}-free HBSS (in mmol l^{-1}: 137.93 NaCl, 5.32 KCl, 0.44 KH_2PO_4, 0.34 $Na_2HPO_4{\cdot}7H_2O$, 5.56 D-glucose; pH 7.5) and lamellae were excised from the cartilage, washed with the same saline and digested with trypsin (HBSS containing 0.5 g l^{-1} of trypsin and 0.25 mmol l^{-1} of EDTA; Invitrogen, Darmstadt, Germany). Digestion was performed on a shaker at room temperature in six 10-min rounds. Cell suspensions from two such rounds were pooled in saline containing Ca^{2+} and Mg^{2+} (HBSS+: HBSS with, in mmol l^{-1}: 1.26 $CaCl_2$, 0.49 $MgCl_2{\cdot}6H_2O$, 0.41 $MgSO_4{\cdot}7H_2O$; pH 7.5) and 10% fetal bovine serum (FBS; Invitrogen) on ice and were centrifuged at 124 ***g*** and 4°C for 5 min. Cells were resuspended in Leibovitz L15 culture medium containing 5% FBS and antibiotics (L15+: 100 i.u. l^{-1} penicillin, 0.1 mg l^{-1} streptomycin, 50 mg l^{-1} gentamycin; Invitrogen) with a final osmolarity of 305 mOsm. This procedure was repeated twice. The resulting three cell suspensions from the six digestions were cultured in Petri dishes (Sarstedt, Nümbrecht, Germany) in a Peltier-cooled incubator (Memmert, Schwabach, Germany) at 18°C and ambient air. After 24 h culture they were washed thoroughly with HBSS+ to remove blood cells and mucus and more L15+ was added. Thereafter cells were washed every 2 days with L15 medium containing 5% FBS, but no antibiotics (L15–).

Five days after isolation cells were trypsinized a second time, washed and seeded onto filter inserts [transparent polyethylene terephthalate (PET) Falcon cell culture inserts for 12-well plates, with a pore size of 0.4 μm; Becton Dickinson, Heidelberg, Germany] at a density of 0.5×10^6 cells per insert. The next day, cells were washed with HBSS+ followed by the addition of L15– on both sides. For experiments including measurement of Phenol Red (PR) diffusion, cells were seeded and held in PR-free L15 medium (Invitrogen).

Cortisol exposure and experimental solutions

Cortisol (cortisol 21-hemisuccinate sodium salt, H2270; Sigma, Munich, Germany) was added to the basolateral side of the inserts at a concentration of 2 μmol l^{-1} in culture medium (1000 ng ml^{-1}) according to a previous published protocol (Kelly and Wood, 2001a). L15 medium (with or without cortisol) was renewed every 24 h.

FW was prepared using deionized water according to the following recipe for 3 mOsm synthetic FW (in mmol l^{-1}: 0.45 $Na_2HPO_4{\cdot}2H_2O$, 0.09 $NaH_2PO_4{\cdot}H_2O$, 0.45 $CaCl_2{\cdot}2H_2O$, 0.05 $MgCl_2{\cdot}6H_2O$; pH 7.5) (Wood and Pärt, 1997). The other saline solutions used in the experiments were based on 3 mOsm synthetic FW with increasing concentrations of NaCl (305 mOsm with 165 mmol l^{-1} NaCl, 770 mOsm with 435 mmol l^{-1} NaCl; pH 7.5). The 305 mOsm solution represented an iso-osmotic solution comparable to the 305 mOsm L15 culture medium. A 770 mOsm solution was chosen to represent a medium strength hyperosmotic saline compared with full SW-strength 1000 mOsm saline, which increased mortality of the cells. Osmolarity of solutions was measured using a freeze-point semi-micro osmometer (Knauer, Berlin, Germany).

TER and PR diffusion (PRD) measurement

TER was measured after culture medium renewal using a normal (20 kΩ) or a custom-modified (200 kΩ) epithelial voltohmmeter (EVOM®; WPI, Berlin, Germany). TER values were transformed

to Ωcm^2 and were corrected for resistance values of blank inserts with apical and basolateral L15 medium (symmetrical) or apical osmotic and basolateral L15 medium (asymmetrical).

Epithelial PRD was measured using a modified approach of Jovov et al. (Jovov et al., 1991). PR is a non-absorbable, non-toxic pH indicator component of many growth media formulations (Lewis, 2002; Rathore et al., 2008), which is also commonly used as a paracellular permeability marker in many epithelial cell studies (Azenha et al., 2004; Paye et al., 2007; Peixoto and Collares-Buzato, 2005). By using high-performance liquid chromatography (HPLC), extremely low concentrations (10 ng ml^{-1}) of the small molecule can be detected (Varma et al., 2004).

1 day before asymmetrical culture started and 1 and 2 days after asymmetrical culture started in symmetrical recovery experiments, the basolateral medium was exchanged for L15+PR (L15 containing 10 mg l^{-1} PR) to start diffusion of PR from the basolateral to the apical side. Twenty-four hours later a 200 µl sample was drawn from the apical insert compartment and immediately frozen for further analysis. Subsequently cultures were washed and the respective saline (or L15 without PR for recovery experiments) was added apically and fresh L15+PR was added basolaterally.

Because PR is a pH indicator its absorbance qualities will change with the pH of the solution. Therefore, prior to measurement, samples were thawed and alkalinized with 2 mol l^{-1} NaOH to eliminate the pH indicator feature of the PR molecule. A volume of 70 µl of the supernatant was analyzed by HPLC using a LiChrospher 60 RP select B column (0.4×5 cm, 5 µm particle size; Merck, Darmstadt, Germany). The mobile phase was 20 mmol l^{-1} KH_2PO_4, pH 6.0, containing 20% acetonitrile. Photometric detection was carried out with an Isco V4 photometer at 434 nm (0.02 absorbance, 10 mm path). PR concentration was calculated using 10, 5, 1 and 0 vol.% of L15+PR medium in iso-osmotic saline (305 mOsm) as standards. PRD data are presented as µmol l^{-1} day^{-1}.

Experimental setups

SSI cultures of each gill cell preparation were cultured for at least 5 days. Cultures with TER values below 2 kΩcm^2 after 5 days in symmetrical culture were not used for an experiment.

Total RNA, for ddPCR analysis and subsequent mRNA quantification, was isolated after 24 h from SSI cultures where the apical medium was either exchanged for synthetic FW or for L15 growth medium (symmetrical control).

For all other experiments, including a second mRNA quantification, we sampled cells from each preparation at three time points. The first, before osmotic stress application, with apical culture medium (symmetrical), was termed 'pre-stress', the second, after 24 h of apical osmotic stress with 3 mOsm or 770 mOsm saline (asymmetrical), was termed '24 h osmotic stress' and the third, after 48 h of recovery with culture medium (symmetrical) from 3 mOsm or 770 mOsm saline incubations was termed '48 h recovery'.

TER and PRD were recorded from the same individual cultures on day 1 (shortly before applying osmotic stress) and day 2 (at the end of 24 h of osmotic stress, before medium change) and, for recovery experiments, on days 3 and 4.

Differential display polymerase chain reaction (ddPCR) and sequence alignment

ddPCR was conducted according to Liang et al. using seven arbitrary 13mer primers in combination with three one-base-anchored oligo(dT) primers (Table 1A) to produce a set of unpredictable PCR amplifications from the 3′ site of cDNA from symmetrical control and FW-incubated cultures (Liang et al., 1994).

Table 1. Primer sequences used for (A) differential display PCR, (B) amplification of the claudin 28b coding region and (C) claudin 28b real-time PCR analysis

Analysis	Sequence
A. Differential display PCR*	
	Arbitrary primers
	A1: 5′-AAGCTTGCACCAT-3′
	A2: 5′-AAGCTTCGACTGT-3′
	A3: 5′-AAGCTTGATTGCC-3′
	A4: 5′-AAGCTTAGAGGCA-3′
	A5: 5′-AAGCTTTCATATG-3′
	A6: 5′-AAGCTTTCCGATA-3′
	A7: 5′-AAGCTTAAGCTTG-3′
	One-base-anchored oligo(dT) primers
	$HT_{11}C$: 5′-AAGCTTTTTTTTTTTC-3′
	$HT_{11}G$: 5′-AAGCTTTTTTTTTTTG-3′
	$HT_{11}A$: 5′-AAGCTTTTTTTTTTTA-3′
B. Amplification of the claudin 28b coding region	
	forward: 5′-TCCATTCTACCAGGGCTCCATCAGG-3′
	reverse: 5′-CAGCAAGGCCTACGTCTAGAGGGTTAGA-3′
C. Real-time PCR analysis	
	forward: 5′-CGACTCCCTCCTGGCCTTAC-3′
	reverse: 5′-GCAATTATGGCGATTATGATCAGA-3′

*Liang et al., 1994.

RNA for subsequent cDNA production was isolated from cells on filter inserts using TRIzol® reagent (Invitrogen) following the manufacturer's instructions. After a DNAse digestion step, RNA concentrations were measured using the Ribogreen kit (Invitrogen) and a plate reader (Victor X4, Perkin Elmer, Rodgau, Germany). 1 µg of total RNA was used for cDNA synthesis with MMLV reverse transcriptase (Promega, Mannheim, Germany) and oligo(dT) primer following the manufacturer's instructions.

ddPCR was conducted at low annealing temperatures with a hotstart enzyme (HotMaster® Taq, Eppendorf, Vienna, Austria). Following a 15 min hotstart at 95°C, 35 cycles of 30 s at 94°C, 1 min at 40°C and 1 min at 70°C were conducted. The amplification program ended with a final elongation for 10 min at 72°C. To reduce false positives in ddPCR, each cDNA was amplified in duplicates with each different primer combination and final products were separated on 6% polyacrylamide gels (3 h at 70 W, ~1850 V, ~38 mA). The gel was silver stained (Bassam et al., 1991) and only bands that could be either found in both of the duplicate control lanes of the gel (gene downregulated) or in both of the duplicate FW lanes (gene upregulated) were excised with a sterile scalpel. Subsequently DNA was eluted for 30 min at 100°C with 50 µl Maxam–Gilbert elution buffer (0.5 mol l^{-1} sodium acetate, 10 mmol l^{-1} magnesium acetate, 1 mmol l^{-1} EDTA, 0.1% SDS) precipitated and finally resuspended in 10 µl nuclease-free water.

DNA from differential bands was reamplified under identical PCR conditions and primers. Reamplified products were cleaned with the Nucleospin® Extract II kit (Macherey-Nagel, Düren, Germany) according to the manufacturer's instructions. Finally, the cleaned PCR products were used as template in a 10 µl cycle sequencing reaction (BigDye® 1.1 Terminator Cycle Sequencing Kit, Applied Biosystems, Foster City, CA, USA) using the appropriate forward or reverse primers from the initial ddPCR. Sequences were acquired on an ABI 373 sequencer (Applied Biosystems).

Finally, sequences were BLAST-aligned to non-redundant nucleotide databases (nr/nt), reference mRNA sequence databases (refseq_rna) and non-human, non-mouse EST databases (est_others) in the NCBI BLAST suite (http://blast.ncbi.nlm.nih.gov). Results

were analyzed using iHOP [http://www.ihop-net.com; information hyperlinked over proteins (Hoffmann et al., 2005)].

Claudin 28b sequence retrieval and antibody design

A 116 bp sequence from the ddPCR approach aligned to claudin e was the starting point to form a 1474 bp contig sequence comprising three clones (GenBank accession nos BX299368, BX887898 and BX299367) from an *Oncorhynchus mykiss* cDNA library.

Validation of the contig alignment was achieved by amplification of a 670 bp fragment in cDNA from trout SSI cultures with PCR using a HotMaster® Taq enzyme (Eppendorf) and primers flanking the coding region (Table 1B) and an appropriate cycle protocol (2 min at 94°C, 35 cycles of 15 s at 94°C, 15 s at 59°C and 1 min at 65°C and a final elongation step of 10 min at 65°C) in a PE Geneamp 9700 cycler (Applied Biosystems). The PCR product was sequenced using Big Dye® Terminator 3.1 in a 3130 Genetic Analyzer (Applied Biosystems).

The last 15 C-terminal amino acids of the claudin protein sequence were used as antigen. Peptide synthesis, standard custom antibody synthesis in two rabbits, and antibody purification was performed by Eurogentec (Seraing, Belgium). The isoform specificity of the antigen sequence was tested with BLAST protein sequence alignment. Antibody specificity was further tested with western blot analysis against isolated trout pavement cell protein.

Western blot analysis of claudin 28b

Trout pavement cells in a confluent layer were trypsinized and the cell solution was centrifuged for 3.5 min at 110 ***g***. The resulting cell pellet was shock frozen in liquid nitrogen and stored in a bio freezer for later use. A volume of 30 µl of the sample was heated to 95°C for 2 min and separated by electrophoresis on a 10% Novex gel with NuPage® MOPS SDS running buffer (Invitrogen) at 200 V for 50 min. Proteins were blotted for 60 min onto an Immunoblot PVDF membrane (Bio-Rad, Munich, Germany) at 25 V in a XCell2 blot module (Invitrogen) using NuPage® transfer buffer.

Nonspecific binding sites were blocked with 1× Tris-buffered saline (TBS; in mmol l^{-1}: 100 Tris-HCl, 150 NaCl; pH 7.5) containing 0.1% Tween 20 (TBS-T) and 5% non-fat dry milk powder for 1 h at room temperature. Anti-claudin 28b antibody (150 µg ml^{-1}) and anti-actin antibody (1:2000, A5060, Sigma) were added in TBS-T containing 5% bovine serum albumin (BSA), and were incubated with the membrane overnight at 4°C. After several washes with TBS-T and incubation of the membrane for 60 min at room temperature with horseradish-peroxidase-linked anti-rabbit secondary antibody in blocking buffer (1:1000), protein bands were visualized with ECL western blotting detection reagents (GE Healthcare UK Ltd, Chalfont St Giles, Bucks, UK) for 2 min and imaged in the Gel Doc XR Molecular Imager (Bio-Rad).

Real-time PCR quantification of claudin 28b mRNA

Total RNA isolation, quality assessment and quantification were carried out as described for the ddPCR procedure. For cDNA synthesis, 360 ng of total RNA was used in a 50 µl reaction setup with random hexamers and MMLV reverse transcriptase (both from Fermentas, St Leon-Rot, Germany) following the manufacturer's instructions. Real-time PCR primer design for trout claudin 28b coding sequence (see Table 1C) was carried out with the Primer Express 3.0 software (Applied Biosystems). Real-time PCR was set up in 20 µl reaction volumes of a mastermix containing 1× SYBR® Green (Applied Biosystems), 900 nmol l^{-1} forward primer, 300 nmol l^{-1} reverse primer, 0.5 µg non-acetylated BSA (Sigma-Aldrich) and 2 µl of each cDNA. Each cDNA was measured in triplicate in 96-well optical reaction plates (Applied Biosystems) with an ABI PRISM 7500 Sequence Detector (Applied Biosystems). Additionally, noRT controls (RNA incubated with random hexamers but without reverse transcriptase in the cDNA synthesis procedure) were measured to rule out possible DNA contamination. mRNA copy number was calculated by plotting the CT values against a standard curve of serially diluted cloned and gene-specific cDNA of known copy number (absolute quantification). Finally, copy numbers were normalized to 10 ng of total RNA.

Immunohistochemistry of SSI cultures and gill filaments

Cells grown on inserts were washed once with phosphate buffered saline (PBS; in mmol l^{-1}: 154 NaCl, 3 $Na_2HPO_4{\cdot}7H_2O$, 1 KH_2PO_4; pH 7.4) and immediately fixed in 2% paraformaldehyde in PBS for 15 min at room temperature. Next, antigen retrieval was performed with cold acetone at –20°C for 5 min (Matter and Balda, 2003). Acetone treatment did not alter phalloidin staining and had no visible detrimental effects on cell morphology. Thereafter, cells were washed and permeabilized with PBS-T (PBS with 0.1% Triton X-100). Nonspecific binding sites were blocked with PBS-T containing 10 mg ml^{-1} BSA following incubation with the primary rabbit anti-trout claudin 28b antibody at a concentration of 150 µg ml^{-1} in PBS-T–BSA overnight at 4°C. Secondary antibody was added at a dilution of 1:200 (TRITC-conjugated swine anti-rabbit immunoglobulin antibody; Dako Cytomation, Glostrup, Denmark) together with the F-actin-selective probe Alexa-Fluor®-488–phalloidin (1:150, Invitrogen) in PBS-T–BSA and was incubated for 1 h at room temperature. Finally, cells were washed and nuclei were stained with Hoechst 33342 for 3 min before three concluding PBS washing steps. The PET membrane holding the cells was excised and mounted in Vectashield® (Vector Laboratories, Burlingame, CA, USA).

Claudin 28b staining in 2 µm serial sections of paraffin-embedded (Paraplast, Fisher Scientific, Vienna, Austria) trout gill arches was carried out after dewaxing of the paraffin sections in a series of xylene and ethanol incubations and a 5 min antigen retrieval step with 1% SDS in PBS, pH 7.3 (Wilson et al., 2000). After 20 min in blocking buffer (T-PBS; 0.1% BSA, 0.05% Tween 20 in PBS, pH 7.4), primary antibody was added for 2 h and secondary antibody for 1 h at 37°C in the same concentrations as for the SSI stainings. Finally, sections were washed and mounted in Vectashield.

Image analysis

Confocal laser scanning images were recorded with a Zeiss LSM 510 (Carl Zeiss MicroImaging GmbH, Jena, Germany) equipped with 63× plan-apochromatic optics, minimum pinhole settings and constant laser intensity. Without knowing the experimental treatment, images from three different areas with the focus on the apical-most green fluorescent cortical F-actin signal of cells in the mucosal layer were chosen, independently of the claudin signal. The region of interest was chosen independently from the claudin signal.

Cell junction fluorescence was quantified with a custom-made program for use in Optimas software (Media Cybernetics, Bethesda, MD, USA). After choosing a starting point and endpoint of a cell–cell junction (Fig. 1A), the luminance profile of the red (Fig. 1B) and the green (Fig. 1C) color channel along each of the perpendicular lines was extracted individually (Fig. 1D). For graphical display both profile arms of four extracted profiles were combined and represent the pixel grayscale value from the junctional center towards the cytosol.

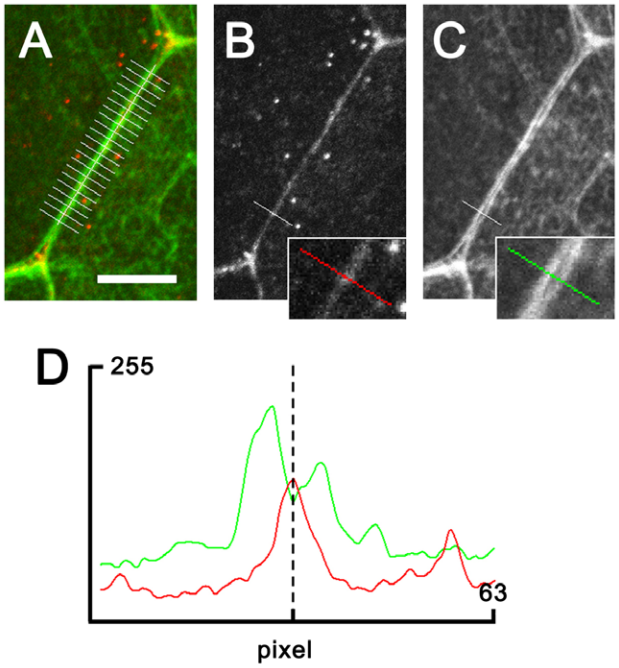

Fig. 1. Quantification of cell junction fluorescence signal. (A) After choosing a starting point and endpoint of a cell–cell junction a series of perpendicular lines were drawn along it. (B–D) The luminance profile of the red (B) and the green (C) color channel along each of the perpendicular lines was then determined and plotted (D). Scale bar, 10 µm.

At the meeting point of three cells in the mucosal layer we occasionally observed a separation of the cells, giving the impression of a pore-like structure. Theses pore-like structures were counted manually using the same set of images as used for cell junction fluorescence quantification. Data are presented as pore-like structures per cm^2 epithelial surface.

Statistics

Values reported in the text and the figures are means ± s.e.m. Experiments were performed in at least three independent cell culture preparations. Differences between control and cortisol-incubated cultures were analyzed using an unpaired two-tailed Student's *t*-test. Differences between osmotic incubations were analyzed by two-way ANOVA with a *post hoc* Holm–Sidak multiple comparison test. The same test was also used to find significant homogenous subgroups at certain fluorescence measurement points at the cell–cell junction. Transformation of data was applied to the dataset of Fig. 11 to meet assumptions for homogeneity and normality. Statistical analyses were performed using Sigmaplot 11.0 (Systat Systems Inc., Chicago, IL, USA). Significant differences were accepted when $P \leq 0.05$.

RESULTS

A trout claudin 28b isoform detected with ddPCR

Besides many reamplified PCR sequences, which coded for microsatellites or unknown sequences, 24 reamplified sequences could be aligned to 17 distinct and annotated genes (see Table 2). Five genes (Table 2, bold) out of the 17 genes could be associated with cell–cell junctions. Based on this analysis we then focused our study on the most prominent of the cell junction-associated proteins, the trout-specific isoform of claudin e. *De novo* sequencing of the PCR product (GenBank accession no. EU921670) confirmed 100% identity to the existing coding sequence obtained from the contig alignment. Owing to the high amino acid sequence similarity to claudin 28b from Japanese puffer fish (*Takifugu rubripes*) and full sequence identity to a partial salmon claudin 28b fragment (GenBank accession no. BK006402 – no C-terminal sequence available) the sequence examined was identified as trout claudin isoform 28b (Fig. 2). Furthermore, the first extracellular loop of trout claudin 28b is highly similar to human claudin 3 and human claudin 4 in its acidic and basic amino acid composition.

Claudin 28b mRNA level

ddPCR detected a reduction in claudin 28b mRNA after 24 h FW incubation compared with cultures that were left in symmetrical culture with apical L15 medium. We could verify this response with real-time PCR. After 24 h FW cultures showed a significantly reduced copy number of claudin 28b mRNA compared with 24 h symmetrical control cultures (23.339±1632 *vs* 30.825±2661 copies per 10 ng total RNA; N=3 or 4, *t*-test with $P \leq 0.05$). We also compared mRNA levels at 2, 8 and 16 h after FW application but did not observe significant differences (data not shown).

In a second experimental run claudin 28b mRNA levels were examined under different osmotic conditions and following cortisol exposure (Fig. 3). Control and cortisol-treated cultures did not significantly differ pre-stress. However, after 24 h in FW and after 48 h recovery from FW in apical L15 medium, cortisol-treated cultures had significantly less claudin 28b mRNA than control cultures. No changes were detected after 24 h incubation in 770 mOsm saline and the respective recovery period (Fig. 3).

Western blot analysis and localization of anti-claudin 28b antibody in SSI culture and in gill sections

Pavement cells cultured on a permeable membrane developed into a single mucosal layer and several serosal layers. In the mucosal layer F-actin and anti-claudin 28b staining were colocalized to an apical perijunctional (cortical) ring whereas in the serosal layers F-actin was arranged in stress fibers and anti-claudin 28b immunoreactivity was absent (Fig. 4). Claudin 28b staining of 2 µm sections of paraffin-embedded trout gill lamellae identified the protein in a punctate pattern at the cell–cell contact region within the surface epithelium (Fig. 5A). A single band of ~22 kDa was present on western blots (Fig. 5C), which corresponds to a molecular mass of 22.3 kDa calculated on the basis of the claudin 28b amino acid sequence. Antigen specificity was further supported by alignment of the 15-amino-acid peptide sequence, used for antibody production, to corresponding regions in gill-specific salmon (*Salmo salar*) claudin isoforms available in databases; however, there were only weak similarities. The best matching salmon claudin 28a shared only seven out of the 15 amino acids.

Claudin 28b fluorescence intensity in the tight junction

Using an image analysis protocol for tight junction fluorescence quantification and an extended experimental protocol (hyperosmotic and iso-osmotic incubation, a 48 h recovery period in growth medium and a cortisol-treated cell culture group), we wanted to characterize the plasticity of claudin 28b and F-actin in the cell–cell contact area under these new conditions. Because of the prominent co-localization of claudin 28b to the cortical F-actin ring we regularly added a phalloidin staining step to the protocol to visualize this ring.

Control cells had a stronger claudin 28b fluorescence intensity than cells that were exposed to cortisol basolaterally (Fig. 6 and Fig. 7A, gray shaded area). After hypo-osmotic stress with 3 mOsm

Table 2. BLAST alignment results of reamplified and sequenced differentially expressed bands

GenBank Acc. no.	Length	With FW	BLAST database	Identities (%)	BLAST result (Acc. no.)	Unigene putative ID (symbol)	BLAST result species
HO056163	315 335	Down	nr/nt nr/nt	255/266 (95%)	BT060025.1	60S ribosomal protein L35a (rpl35a)	*Salmo salar*
HO056164				194/254 (76%)			
HO056170	181	Down	nr/nt	108/116 (93%)	BT059338.1	L-lactate dehydrogenase B chain (ldhb)	*Salmo salar*
HO056168	161	Down	nr/nt	108/126 (85%)	BT074643.1	ras-related protein Rab-6B (rab6b)	*Osmerus mordax*
HO056165	547	Down	nr/nt	494/509 (97%)	BT043744.1	ribosomal protein L12 (rpl12)	*Salmo salar*
HO056160	254	Both*	nr/nt nr/nt	55/62 (88%)	XM_002762087.1	**actinin, alpha 4 (actn4)**	*Calithrix*
HO056161	236			67/79 (84%)			*jacchus*
HO056176	382	Down	nr/nt	284/335 (84%)	BT056943.1	**four and a half LIM domains protein 1 (fhl)**	*Salmo salar*
HO188872	174 181	Up	nr/nt nr/nt	132/132 (100%)	NM_001160603.1	NADH dehydrogenase 1 beta	*Oncorhynchus*
HO056169				81/87 (93%)		subcomplex subunit 10 (nduba)	*mykiss*
HO056166	267 249	Down	nr/nt nr/nt	184/195 (94%)	BT058833.1	ras GTPase-activating protein-binding	*Salmo salar*
HO056167				154/166 (92%)		protein 2 (g3bp2)	
HO056175	437 408	Down	nr/nt nr/nt	177/188 (94%)	NM_001160695.1	cornichon homolog 4 (cnih4)	*Oncorhynchus*
HO056174				48/58 (82%)			*mykiss*
HO056162	343	Up	nr/nt	182/222 (81%)	BT057599.1	H/ACA ribonucleoprotein complex subunit 4, dyskerin (dkc1)	*Salmo salar*
HO056159	251	Down	nr/nt	87/117 (74%)	NM_018027.3	**FERM domain containing 4A (frmd4a)**	*Homo sapiens*
HO056183	255 241	Both*	nr/nt	79/102 (77%)	EG832133.1	eukaryotic translation initiation factor 4,	*Danio rerio*
HO056186			est_others			gamma 2a (eif4g2a)	
HO056182	319	Down	est_others	273/278 (98%)	GE825673.1	selenoprotein X,1 (sepx1)	*Danio rerio*
HO056152	560 259	Down	est_others	86/97 (88%)	BX299367.3	**claudin e (cldne)**	*Danio rerio*
HO188873			est_others	101/106 (95%)			
HO188874	361	Up	est_others	95/100 (95%)	CA347340.1	40S ribosomal protein S16 (rps16)	*Oncorhynchus* *mykiss*
HO056155	185	Up	refseq_rna	92/122 (75%)	NM_001124418.1	**clusterin-1, apolipoprotein j (clu)**	*Oncorhynchus* *mykiss*
HO056187	324	Up	est_others	258/285 (90%)	BX863519.3	transcription factor 7-like 2 (tcf7l2)	*Homo sapiens*

Bold type indicates the gene products known to be involved in the plasticity of the epithelial cell–cell contacts.
Note that some re-amplified ddPCR products coded for sequences that aligned to the same gene.
*Two genes were both upregulated and downregulated after 24 h exposure to freshwater, depending on the ddPCR amplification.

saline, tight junction fluorescence of claudin 28b was significantly stronger than after hyperosmotic stress with 770 mOsm saline.

In cortisol-treated cells, claudin fluorescence intensity did not change after 24 h of osmotic stress and showed a similar, weak and partly discontinuous fluorescence signal as that already observed in pre-stress cultures. However, quantitative analysis revealed that in the presence of cortisol recovery from hypo-osmotic stress increased claudin 28b fluorescence significantly (Figs 7 and 8). Finally, incubation with iso-osmotic saline (305 mOsm) did not significantly change claudin tight junction fluorescence intensity compared with pre-stress values in control or cortisol-treated cultures (data not shown). A schematic overview of significant fluorescence level difference, calculated at the center of the tight junction, is presented in Fig. 7B.

F-actin fluorescence intensity in the tight junction

The fluorescence intensity of the cortical F-actin ring was similar in control and cortisol-treated cultures (Fig. 6 and Fig. 7A) and fluorescence intensity did not significantly change after iso-osmotic saline application (data not shown). Hypo-osmotic stress for 24 h led to significantly stronger F-actin fluorescence at the tight junctions of control cultures (grayscale value: 165±4, all treatments N=5) compared with pre-stress values (127±6) and hypo-osmotically incubated cortisol-treated cultures (117±7). Recovery from low osmotic stress, however, did not reduce the fluorescence intensity within the observed time frame.

In cortisol-treated cultures recovery from hypo-osmotic stress increased junctional F-actin (Figs 7 and 8). Similarly, F-actin fluorescence of cortisol-treated cultures was significantly increased under 770 mOsm saline stress compared with pre-stress values. With recovery from high osmotic stress, F-actin fluorescence in cortisol-treated cells was reduced compared with post-stress values (Figs 7 and 9).

In control cells under 770 mOsm hyperosmotic stress, many of the adjacent perijunctional F-actin rings were found to separate (Fig. 9) and the density of pore-like structures (see below) in contact areas of three cells increased. Re-establishment of apical culture medium reversed these processes.

Density of pore-like structures in tricellular junctions

In the mucosal cell layer we occasionally detected pore-like-structures at the meeting point of three cells, at densities between 350 and 5000 pore-like structures per cm^2 (Figs 8 and 10). The images gave the impression that the cells separated exactly at the meeting point, and around an unstained center a ring of colocalized anti-claudin 28b and F-actin staining, with a diameter of ~2–5 μm, was observed. There were significantly more of these structures in control than in cortisol-treated cultures during incubation in 770 mOsm saline and after 48 h of recovery from 3 mOsm saline (Fig. 10). The difference after the 770 mOsm incubation leveled off after 48 h of recovery with L15 medium. Under iso-osmotic saline incubation (305 mOsm) pore-like structure density was in the range of pre-stress and 3 mOsm values and results for control and cortisol-treated cultures were not significantly different (control: 2.337±402, cortisol-treated: 2.077±328 pore-like structures per cm^2; N=6; data not shown).

TER and PRD – pre-stress, osmotic stress and recovery

SSI cultures developed high resistance pavement cell epithelia with low PRD (Fig. 11). Continuous treatment with cortisol significantly increased epithelial tightness.

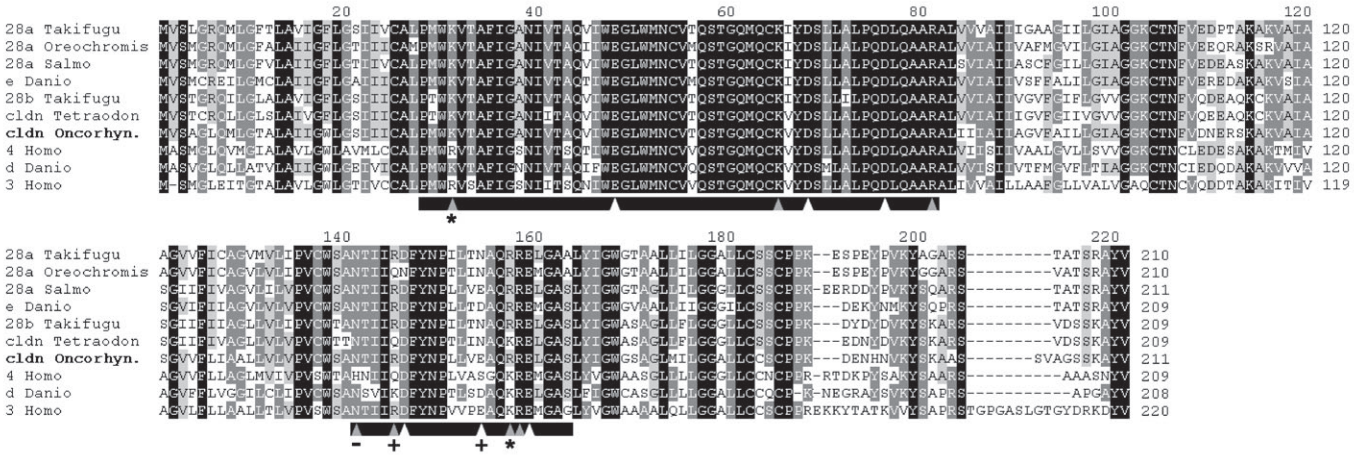

Fig. 2. Claudin isoform alignment. Amino acid alignment (100, 80 and 60% sequence identity of conserved regions represented by black, dark gray and light gray shading, respectively) of the translated coding region of the trout claudin contig sequence (bold) to other fish claudin sequences (some unnamed), retrieved by BLASTP searches, and human claudin 3 and 4 isoforms (3 *Homo* and 4 *Homo*). Black bars mark the two extracellular loops that are believed to form an ion-selective pore with basic and acidic amino acids (gray and white arrowheads, respectively). Sequence differences between trout claudin (cldn *Onchorhyn.*) and human claudins (*Homo*) show neutral differences (*) in both human isoforms 3 and 4 and loss (–) and addition (+) of acidic and/or basic amino acids in human isoform 4 only.

After 24 h of hypo-osmotic stress (3 mOsm) TER and PRD in control and cortisol-treated cultures were not significant different compared with the pre-stress values. Cortisol-treated cultures had still higher TER and lower PRD values compared with respective control cultures.

Compared with the respective pre-stress values, hyperosmotic incubation (770 mOsm) significantly reduced TER (0.16±0.01 and 0.36±0.07 kΩ cm^2) and increased PRD in control and cortisol-treated cultures, respectively. After 24 h exposure to 770 mOsm saline, PRD was still significantly lower when cortisol was present. Control cultures, incubated with iso-osmotic saline (305 mOsm), did not change TER or PRD compared with pre-stress cultures.

After 24 h recovery, TER of cultures that were previously subjected to 770 mOsm were significantly increased, whereas TER of cultures that had been exposed to FW decreased. After 48 h of recovery, control cultures were significantly higher in their TER and lower in their PRD values compared with cortisol-treated cultures independent of whether the initial osmotic stress was hypo-osmotic or hyperosmotic (Fig. 11). Furthermore, PRD of control cultures returned to the original pre-stress value, whereas PRD of cortisol-treated cultures failed to do so, again independent from the initial type of osmotic stress.

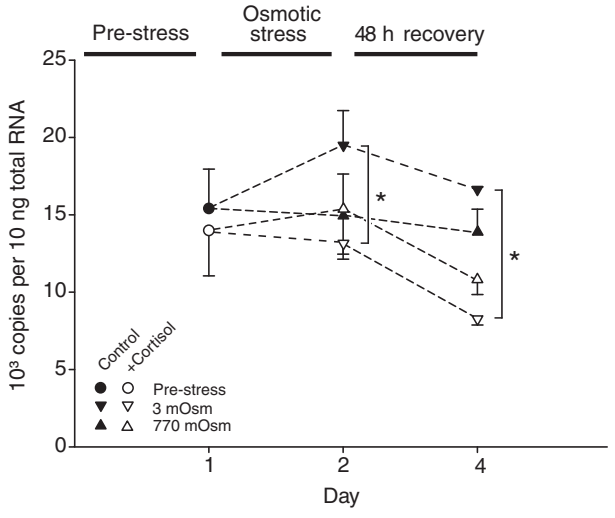

Fig. 3. Claudin 28b mRNA quantification. Claudin 28b mRNA response to 24 h apical incubation with 3 mOsm or 770 mOsm saline and after a subsequent 48 h recovery in L15 medium compared with the pre-stress level, in control (black) and cortisol-treated (white) cultures. The dashed line indicates that data points are from independent samples. *Significant differences ($P \leq 0.05$, ANOVA and a Holm–Sidak multiple comparison test). Values are means ± s.e.m., N=4–6.

DISCUSSION

Critique of methods

In our experiments we created hypertonic challenges by using various concentrations of NaCl in synthetic FW. Although NaCl is the principal determinant of tonicity in the extracellular fluid and in SW, it would be necessary to use non-permeating sugars such as mannitol or sorbitol to validate the pure hypo- or hypertonic portion of the applied stress (Burg et al., 2007). NaCl also induces ionic stress. But NaCl is the main osmolyte in SW and therefore fish migrating between SW and FW do experience NaCl changes. In this respect the 770 mOsm saline represented conditions more physiological than exposure to an artificial osmolyte such as mannitol or sorbitol, which the cells will never experience in nature. Using synthetic or natural SW, besides the change in NaCl concentration, would have also caused changes in other ionic factors, e.g. Ca^{2+} and Mg^{2+} and thus would have made the interpretation of the data even more complex. Therefore, the results of hyperosmotic exposure obtained in this study do not represent a response to a SW-like environmental stress but rather address the effects of increasing or decreasing NaCl concentrations in an artificial culture system. In this way the results of this study may characterize the impact of NaCl concentration as one aspect of SW adaptation. The fact that iso-osmotic saline (305 mOsm) did not significantly alter many of the parameters we looked at compared with symmetrical control conditions may support our approach.

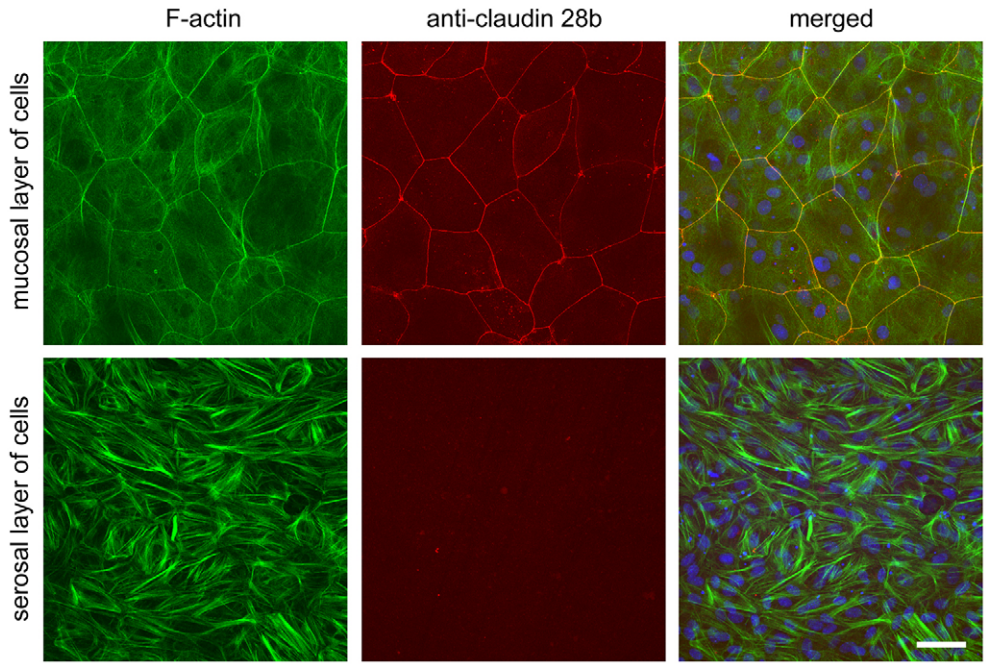

Fig. 4. Immunohistochemical analysis of gill cells on permeable support in symmetrical culture. (A) Triple staining of cultures for F-actin with Alexa-Fluor-488–phalloidin (green), for tight junctions with an anti-claudin 28b antibody (red) and for cell nuclei with Hoechst 33342 (blue). Images represent vertical projections of image stack slices one to five (cells in mucosal layer) and 10–13 (cells in serosal layers). A *z*-projection side-view revealed that the cell culture was only ~10–15 μm high. Note the colocalization of F-actin and claudin 28b in the cell–cell contact areas and the absence of such structures in cells of the serosal layers. Scale bar, 50 μm.

mRNA expression changes of tight junction proteins

Several studies have successfully used ddPCR to identify novel transcripts involved in fish osmoregulation (Pan et al., 2002; Pan et al., 2004; Sakamoto et al., 2000; Suzuki et al., 1999). In our study most of the sequences identified with ddPCR were previously unknown in gill FW adaptation (Table 2). The fact that after 24 h of apically applied FW five transcripts identified with ddPCR were associated with the cytoskeleton and tight junctions highlights the dynamic role of the cell–cell contacts and also the adaptational importance of pavement cells in general. These transcripts include: a homolog of claudin e, an integral part of the tight junction; clusterin-1, a stress response chaperone (Warskulat et al., 2001; Wiggins et al., 2003) restoring tight junctions (Kim et al., 2007); FERM domain-containing 4A, a protein that has important actin-binding domains and possible involvement in apical protein targeting (Rasmussen et al., 2008); α-actinin 4, a stress-related actin–tight junction cross-linking protein (Michaud et al., 2006; Patrie et al., 2002); and four and a half LIM domains, a transcription factor

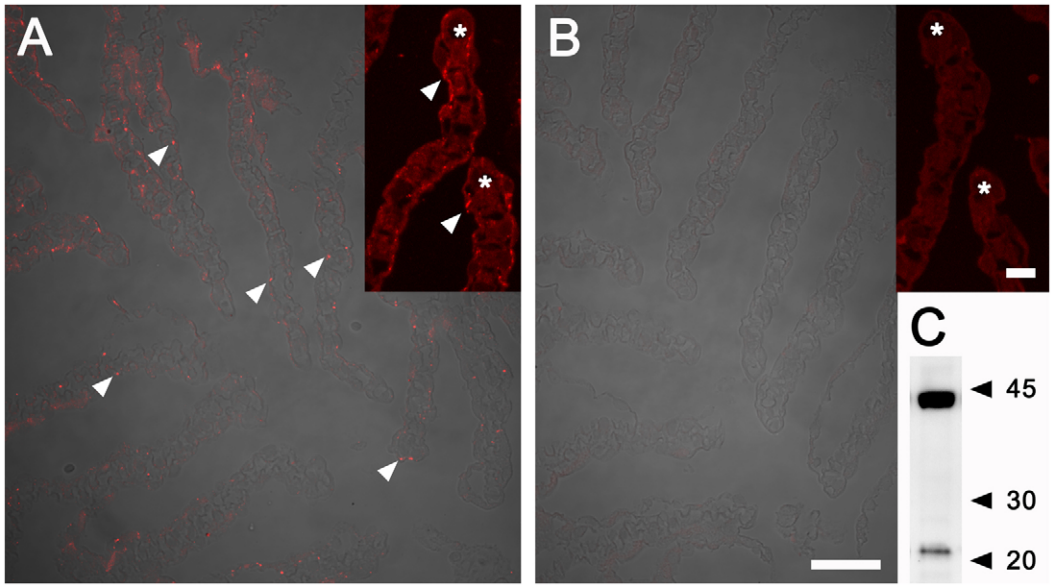

Fig. 5. Anti-claudin 28b reactivity in sections of rainbow trout gill lamellae and in a western blot. The red fluorescence signal of anti-claudin 28b reactivity was superimposed onto phase contrast images of trout gill lamellae. (A) Staining for claudin 28b is present on the mucosal side of the lamellae in the area of the cell–cell contact (arrowheads). Note that staining can be found at the base as well as at the tip of individual lamellae. The insert shows details of the staining in two lamellae where tips are marked with an asterisk. Scale bar, 10 μm. (B) Staining was not present in negative controls where the primary antibody was omitted. Scale bar, 25 μm. (C) Western blot analysis of protein from trout pavement cells, which had been cultured on a solid support, probed with anti-claudin 28b antibody and anti-actin antibody. Besides a 44 kDa band for actin an ~22 kDa protein was identified (numbers correspond to kDa rainbow marker).

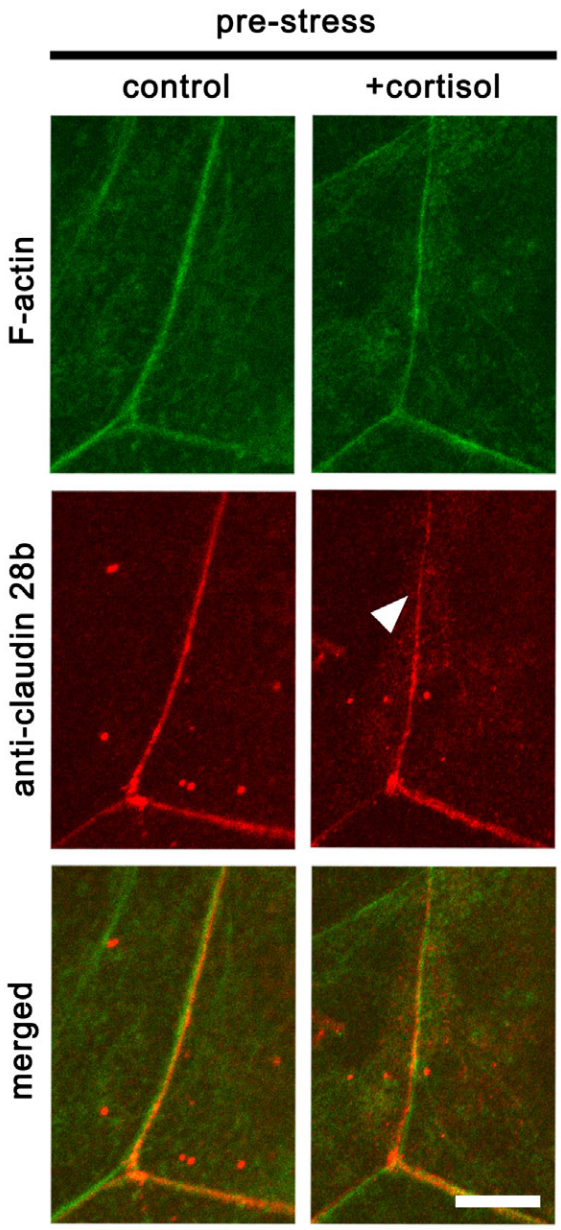

Fig. 6. Cell junctions of control and cortisol-treated cells in symmetrical L15 culture before apical osmotic stress. Control (left) and cortisol-treated (right) cells were stained for F-actin with Alexa Fluor 488 (green) and for tight junctions with a trout-specific anti-claudin 28b antibody (red). Images show typical details of areas in the apical-most focus plane where three cells of the mucosal layer meet. Note the reduction of anti-claudin signal in cell junctions of cortisol-treated cultures (arrowhead). Scale bar, 10 μm.

involved with actin stress fibers at the cell junction (Mistry et al., 2004; Shen et al., 2006b). The rest of the identified transcripts were involved in general stress response, protein synthesis control or metabolism.

We chose the claudin isoform for further investigation because claudins together with occludin and junctional-adhesion molecule (JAM) constitute the zonula occludens, the tight junction of chordates (Tsukita et al., 2001). In addition, a gill-specific function of claudin 28b was warranted by the fact that this isoform is mainly expressed in gill tissue of puffer fish (Loh et al., 2004) and salmon (Tipsmark et al., 2008b).

ddPCR analysis showed a decrease in claudin 28b mRNA level after 24 h of apically applied FW compared with an incubation with apical growth medium (symmetrical control). We could verify this result with real-time PCR analysis, however, compared with symmetrical pre-stress mRNA levels in the extended real-time experiment no reduction in claudin 28b mRNA could be seen after 24 h FW. We suspect the known variability of SSI cultures between different cell culture preparations (Wood et al., 2002a) and the apical growth medium exchange in controls of the first experiment, which was not part of the second experimental setup, to have caused this conflict.

Cortisol addition also reduced claudin 28b mRNA in FW-incubated cultures (~40%) compared with control cultures incubated with FW (Fig. 3). This result is in contradiction to the results of Tipsmark et al. who found claudin 28b to be downregulated within 24 h in Atlantic salmon (*Salmo salar*) transferred from FW to SW (a hyperosmotic stress), and Tipsmark et al. who found no response of gill explants of FW Atlantic salmon to cortisol (Tipsmark et al., 2008b; Tipsmark et al., 2009). We looked at NaCl stress in primary cultures of trout pavement cells, but Tipsmark and co-workers looked at SW and whole gill explants of Atlantic salmon. Furthermore, the combination of FW stress and cortisol was not tested in the study by Tipsmark et al. (Tipsmark et al., 2009). Therefore differences in the experimental setup may be the reason for the differences to our results, but there may also be species-specific differences in the response of claudins to osmotic stress.

Interestingly, none of the various treatments used in the studies of Tipsmark et al. and our present investigations resulted in an increase in the expression of claudin 28b mRNA. Thus, claudin 28b may also be regulated at the protein level (Tipsmark et al., 2008b; Tipsmark et al., 2009).

Claudin 28b distribution in multilayered cultures

In a current model of the function of claudin the two extracellular domains of the protein dimerize with extracellular claudin domains of a neighboring cell in homomeric or heteromeric fashion and form ion-selective pores in the intercellular lateral space (Angelow et al., 2008). The gate function of claudin protein, i.e. its ability to limit paracellular passage of water, ions and small solutes, is dependent on the first extracellular loop (Colegio et al., 2003). The basic and acidic amino acid residues in the first extracellular loop of trout claudin 28b showed a high degree of homology to human claudin 3 and human claudin 4. In MDCK (Madin-Darby canine kidney) cell layers the number of strands (Sonoda et al., 1999) and also intensity of anti-claudin 4 fluorescence located in tight junctions could be positively correlated to TER, and in addition, upregulation of claudin 4 in MDCK-II cell cultures caused an increase in TER and decreased sodium permeability (Van Itallie et al., 2001).

Based on these results, we therefore hypothesized that a change in epithelial tightness in our cultures should be associated with a change of claudin 28b fluorescence in tight junctions.

Claudin 28b tight junction fluorescence correlates with epithelial tightness

After 24 h of hypo-osmotic stress, TER in controls was unchanged compared with pre-stress values. This is in line with several other studies (Gilmour et al., 1998; Kelly and Wood, 2001a; Kelly and Wood, 2001b). Also PRD was unchanged after 24 h exposure to FW. A similar result was also obtained for PEG (polyethylene glycol) permeability in one study (Gilmour et al., 1998), whereas PEG permeability was found to double in two other studies (Kelly and Wood, 2001a; Kelly and Wood, 2001b). In line with our

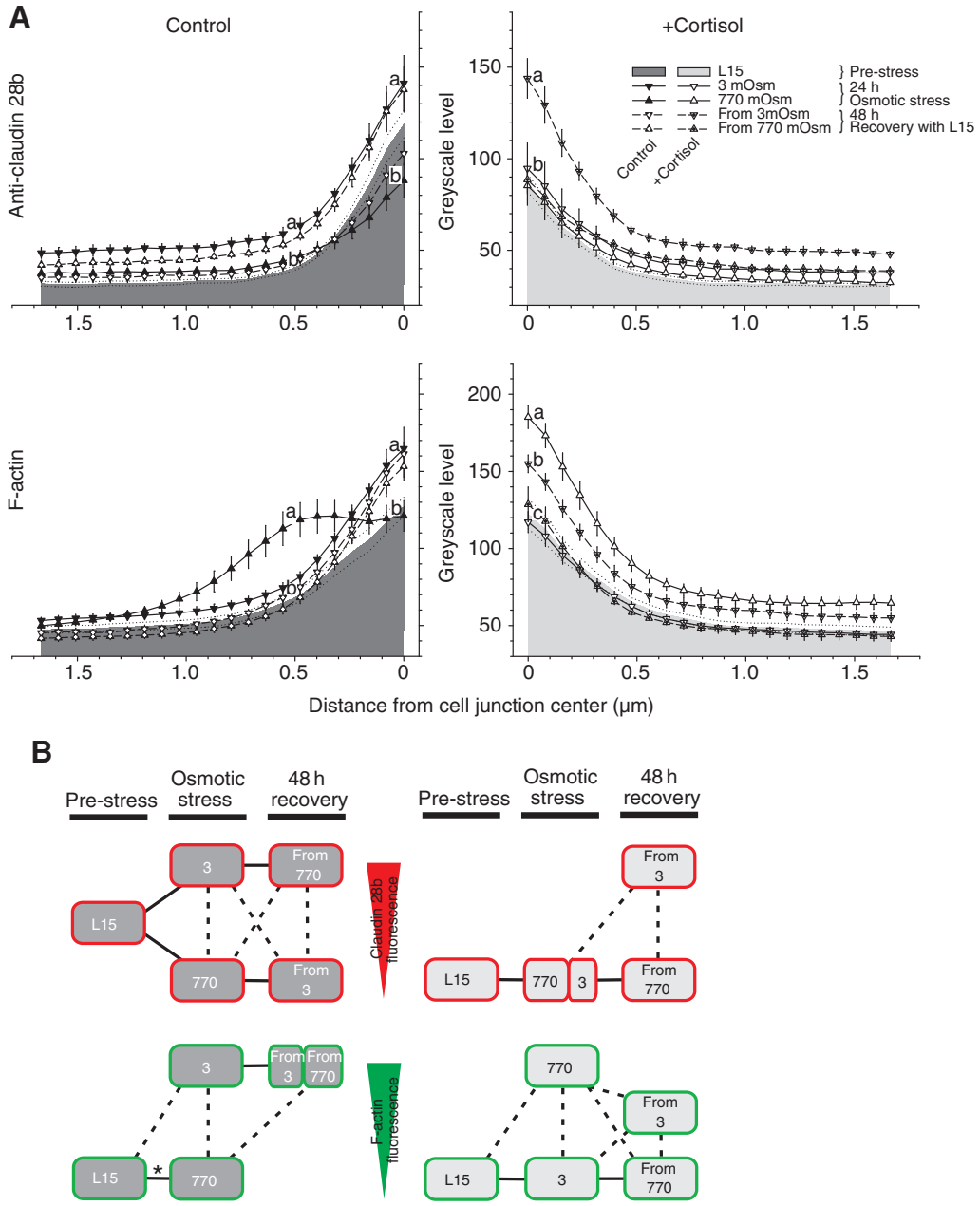

Fig. 7. Comparison of anti-claudin 28b and F-actin fluorescence intensity in cell junctions of control (left column) and cortisol-treated cells (right column) after 24 h osmotic stress and 48 h recovery. (A) Plots represent the pixel grayscale value from the junctional center towards the cytosol (see text and Fig. 1). The gray shaded areas are the mean pre-stress fluorescence intensity in cell junctions; dotted lines indicate ± s.e.m. Recovery data are indicated by dashed lines and filled symbols. Note the reversible separation of two cortical actin strands after hyperosmotic stress in control cells (decentralized peak in the left lower graph) and the reversible significant increase of F-actin signal when cortisol-treated cultures experienced hyperosmotic stress (right lower graph). Significant differences ($P \leq 0.05$) between homogenous subgroups (a, b, c…) were calculated with ANOVA and a multiple comparison test (Holm–Sidak). Values are mean ± s.e.m., $N=4$ or 5. (B) Schematic relationships of significant differences at the center of anti-claudin 28b (red) and F-actin (green) tight junction fluorescence histograms of control (left, dark gray) and cortisol-treated (right, light gray) cultures. Data from symmetrical pre-stress cultures (L15), from 24 h 3 mOsm and 770 mOsm saline-incubated (3 and 770) and from 48 h symmetrical recovery cultures (From 3 and From 770) are shown. A solid line represents no significant difference, whereas a dotted line represents a significant increase or decrease. Note that the significant separation of F-actin strands after 770 mOsm saline is not visible at the junctional center (*).

observations on TER, claudin 28b fluorescence in the tight junction was unchanged compared with pre-stress values.

Because the level of TER in most of our SSI cultures was higher than reported previously (Gilmour et al., 1998; Kelly and Wood, 2001a; Kelly and Wood, 2002; Wood and Pärt, 1997; Wood et al., 1998; Wood et al., 2002b) it seems likely that the tighter the epithelium was prior to hypo-osmotic exposure, the smaller were TER and PRD variances upon hypo-osmotic stress and the more the epithelium was able to retain tightness and claudin 28b protein localization to the tight junction throughout the FW stress. Wood et al. also described how low TER preparations had greater sensitivity to disturbances than high TER preparations (Wood et al., 2002a). This may explain the response of epithelia that experienced a decrease in osmolarity from 770 mOsm to 305 mOsm L15 (48 h recovery from 770 mOsm), where a strong increase in TER and PRD and an increase in claudin 28b tight junction fluorescence intensity coincided.

Hyperosmotic stress, in turn, reversibly reduced barrier properties, and the observed decrease in epithelial barrier tightness was well in the range of cultured gill epithelial cells of tilapia (*Oreochromis niloticus*) including MR cells, where TER decreased from 6–8 kΩ cm^2 under symmetrical conditions to 0.10–0.15 kΩ cm^2 after 24 h of apically applied SW (Zhou et al., 2005). The strong reduction of barrier tightness during hyperosmotic stress was accompanied by a reduction and partial disruption of claudin 28b fluorescence in the perijunctional F-actin ring. Similarly, increasing the osmolarity from FW to 305 mOsm L15 (48 h recovery from 3 mOsm) decreased claudin 28b fluorescence in control cultures significantly, which was in line with reduced TER values. In airway epithelial cells hyperosmotic exposure decreased claudin-4 in the tight junctions as well (Nilsson et al., 2007).

These results reveal that claudin 28b protein distribution was responsive to osmolarity changes and support the conclusion that claudin 28b contributes to epithelial tightness.

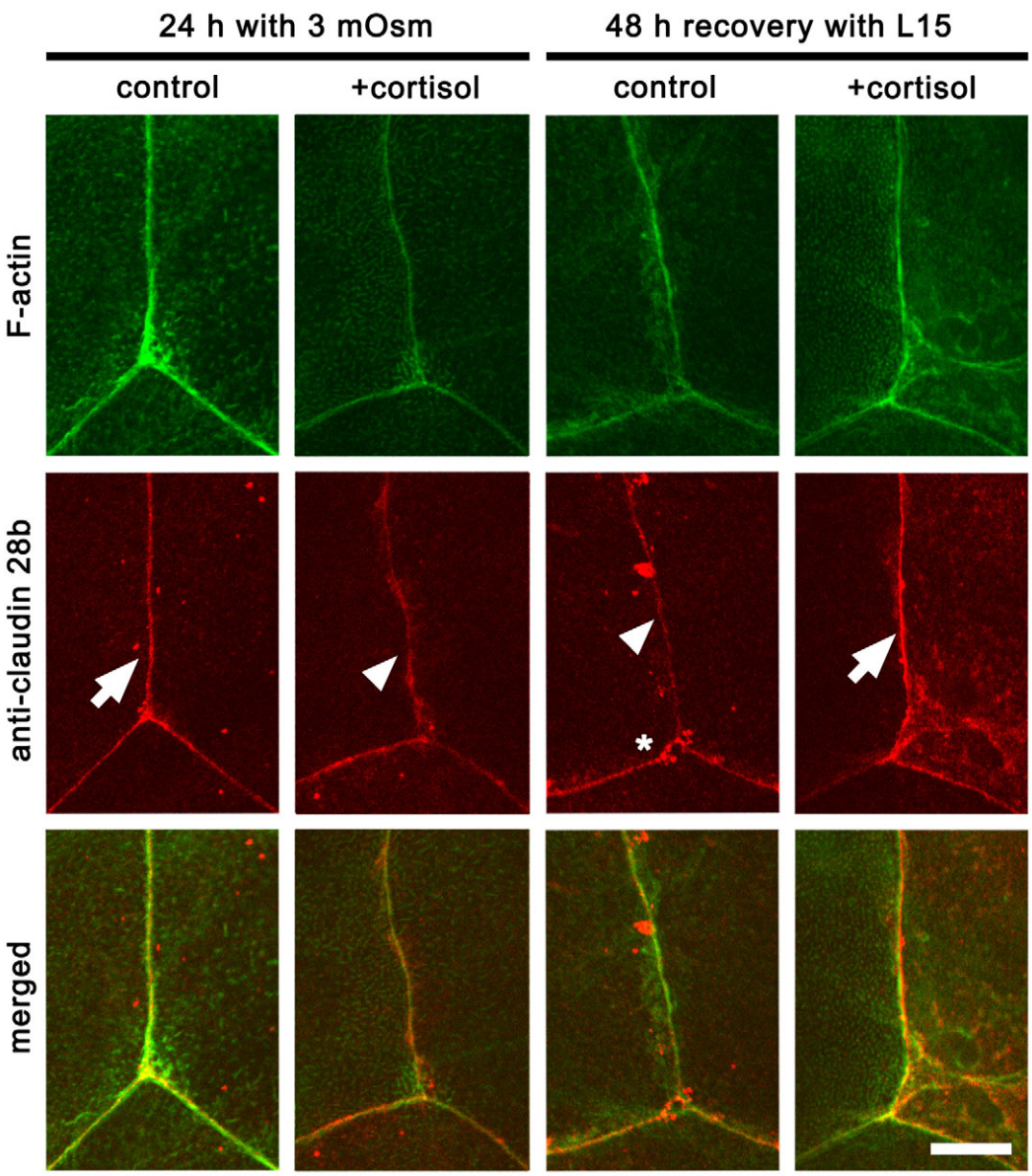

Fig. 8. Cell junctions of control and cortisol-treated cultures after apical hypo-osmotic stress. Control (columns 1 and 3) and cortisol-treated (columns 2 and 4) cultures were incubated with 3 mOsm saline on the apical side for 24 h and, for recovery experiments, were incubated with apical L15 for another 48 h. Note the prominent F-actin signal and the precise anti-claudin 28b colocalization in the junctional region (arrow). Note also the reduction of anti-claudin 28b signal in cell junctions (arrowhead) and the formation of a pore-like structure as well as anti-claudin-28b-reactive particles in the vicinity of the pore-like structure (asterisk). Scale bar, 10 μm.

F-actin distribution is altered in response to hyperosmotic stress

In all preparations claudin 28b colocalized with cortical F-actin in the mucosal cells layer. Cortical F-actin forms a belt around each cell in the epithelial layer and supports the apical junction, similar to the situation observed in the gill epithelium *in situ* (A.M.S., J. Farkas, W. Salvenmoser and B.P., unpublished observation). This arrangement is often referred to as the perijunctional F-actin ring. It was shown in several studies that rearrangement or internalization of tight junction protein caused reduced TER, increased permeability to small solute molecules and was accompanied by a reduction in the intensity of perijunctional F-actin ring fluorescence (Shen et al., 2006a; Shen and Turner, 2005). Accordingly, in our studies the strong F-actin fluorescence in the tight junction of control cultures observed after 24 h of exposure to FW coincided with an unchanged TER, PRD and claudin 28b fluorescence.

After 24 h hyperosmotic stress, cortical F-actin rings of many adjacent cells were separated whereas F-actin fluorescence was not reduced but was still present in solid and continuous single strands (Fig. 9). This separation of cortical F-actin rings was caused by hyperosmotic cell shrinkage because adding stronger saline (970 mOsm) increased the distance between single strands (data not shown). However, in a study on bovine brain microvessel endothelial cells subjected to hyperosmotic urea (Dorovini-Zis et al., 1987), severe cell shrinkage ultimately destroyed tight junction morphology, through membrane retraction, and led to epithelial damage. We never observed epithelial damage after 24 h hyperosmotic stress, and claudin 28b in our study was still localized to the tight junction in a single strand, although with reduced fluorescence intensity and partly disrupted. In fact, with reintroduction of apical iso-osmotic culture medium ring separation was completely reversed and claudin 28b fluorescence was increased at the tight junction. These observations indicate that pavement cell layers can sustain cell shrinkage without losing cell–cell contact at their tight junctions. Therefore, F-actin ring separation does not appear to be a pathophysiological phenomenon, but weakening or opening the contact to tight junction proteins may allow for a modification in claudin 28b distribution in tight junctions (Fanning, 2001).

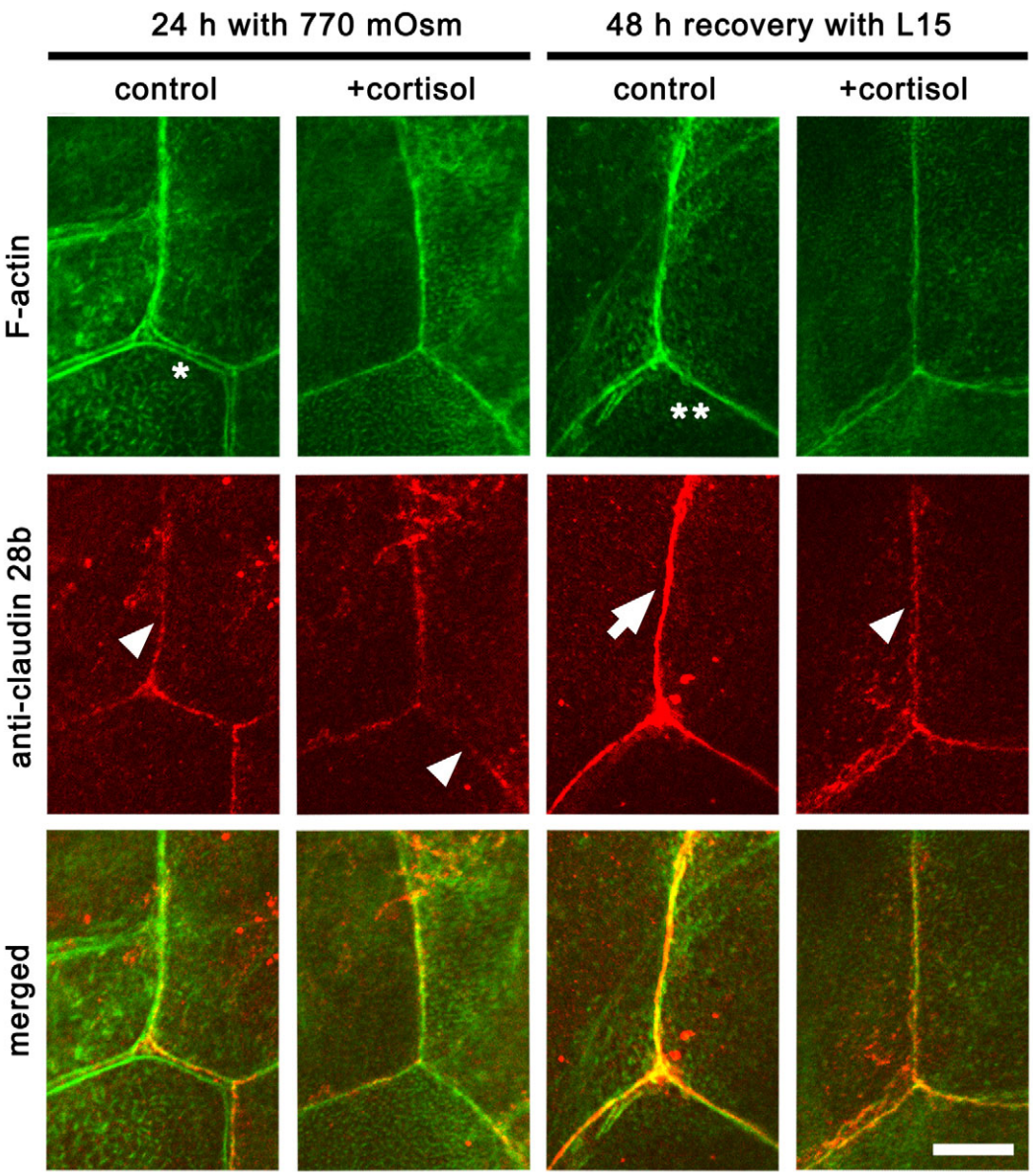

Fig. 9. Cell junctions of control and cortisol-treated cultures after apical hyperosmotic stress. Control (columns 1 and 3) and cortisol-treated (columns 2 and 4) cultures were incubated with 770 mOsm saline on the apical side for 24 h and, for recovery experiments, were incubated with apical L15 for another 48 h. Note the separation of two F-actin strands (asterisk) and the lack of such separations in junctions following recovery (double asterisk). Note also the strong and continuous (arrow) and reduced and discontinuous (arrowhead) anti-claudin 28b signal in the junctional area. Scale bar, 10 μm.

Hyperosmotic F-actin ring separation in our study coincided with the appearance of a larger number of pore-like structures at the meeting points of three cells (tricellular junctions) in control cultures than in cortisol-treated cultures (Fig. 8). Around the unstained center of this structure a colocalized ring of anti-claudin 28b and F-actin staining with an ~2–5 μm diameter was observed. This could indicate that the claudin will subsequently be removed from the membranes, an explanation that is supported by the presence of claudin 28b-stained particles in the vicinity of pore-like structures (Fig. 8). It could also indicate that a cell from underneath replenished the upper cell layer, and this cell did express claudin. However, none of our images showed any sign of new cells within this pore-like structure; the center was always completely dark. These pore-like structures resembled apical crypts in the opercular membrane of *Fundulus heteroclitus* in size (~2–4 μm), in their location (tricellular junctions) but not in density (three to 17 times less) (Daborn et al., 2001). These structures also resembled phalloidin-stained apical crypts in the gill surface of tilapia (*Oreochromis mossambicus*) larva in size (~2 μm) and in location (Tsai and Hwang, 1998). Apical crypts are predominantly found in gill epithelia of fish living in hyperosmotic environments, where they regulate the exposure of underlying chloride cells. If the pore-like structures observed in our study are indeed comparable to apical crypts, this would imply that opening and closing of the pore is solely dependent on the apico-basolateral osmolarity gradient without additional involvement of underlying MR cells, because the epithelium used in our study consisted exclusively of pavement cells. Clearly, *in vivo* apical crypt formation and function has to depend on the communication between pavement cells and MR cells to ensure proper spatial alignment.

In the study by Daborn et al. it was shown that closing of apical crypts in response to hypo-osmotic stress decreased conductance of the epithelium, and was prevented by selective disruption of the actin cytoskeleton with cytochalasin D but not with actin-stabilizing agents or by disruption of microtubules (Daborn et al., 2001). This suggests that apical crypts and the contraction or stabilization of cortical F-actin rings are functionally connected.

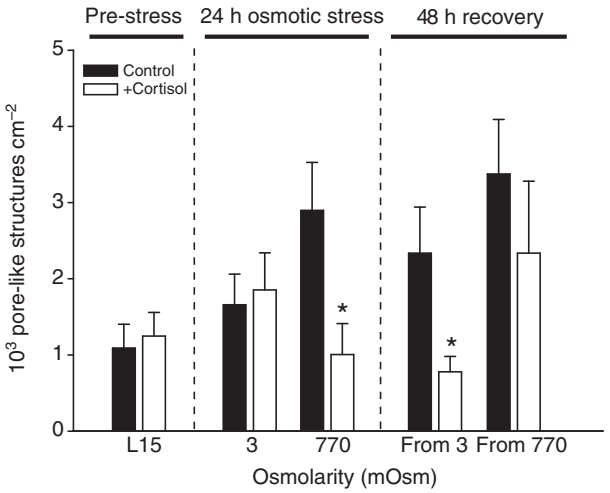

Fig. 10. Quantification of pore-like structures in the mucosal layer of cells. Laser scanning microscopy images of the apical surface were used to count the number of pore-like structures at the meeting point of three cells. Significant differences ($P \leq 0.05$, *t*-test) in pore-like structure number between control (black) and cortisol-treated (white) cultures are shown (*) but no significant differences within control or cortisol-treated cultures were found with ANOVA and a multiple comparison test (Holm–Sidak). Values are means ± s.e.m., N=5–7.

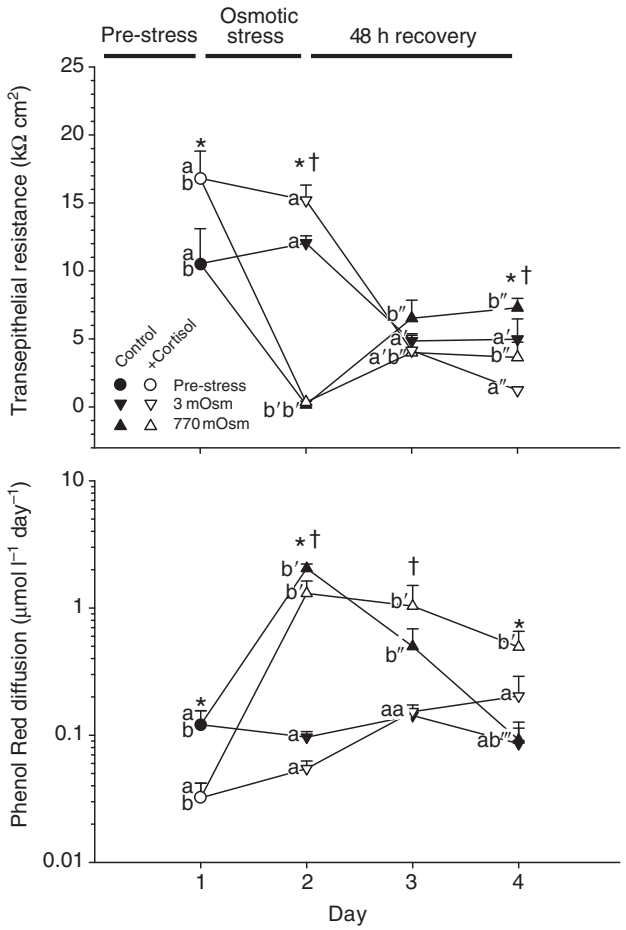

Fig. 11. Recovery of epithelial tightness after osmotic stress. Individual control (black) and cortisol-treated (white) cultures were probed for transepithelial resistance (TER; top) and Phenol Red diffusion (PRD; bottom, note the logarithmic scaling for clarity) over a 4-day period. On day 1 apical L15 medium was exchanged for 3 mOsm or 770 mOsm saline for 24 h. Thereafter, apical L15 medium was restored for 48 h for cells to recover. For every time-point, significant differences ($P \leq 0.05$) between controls and cortisol incubated cultures (*) or between 3 mOsm and 770 mOsm treatment (†) were calculated with two-way ANOVA and a multiple comparison test (Holm–Sidak). The same lowercase letter and number of primes indicates no significant change (e.g. b″, b″) whereas additional primes indicate significant change (e.g. a, a′) between two consecutive timepoints (e.g. day 1 *vs* day 2) of each individual treatment (3 mOsm, 770 mOsm) and culture group (control, +cortisol). Values are means ± s.e.m., N=3–5.

Cortisol increased F-actin under hyperosmotic stress

In the presence of cortisol, ring separation and pore formation after 770 mOsm hyperosmotic stress were absent or reduced, respectively, and cortical F-actin fluorescence in immunohistochemical images was increased compared with cells that experienced FW or had recovered from hyperosmotic stress (Fig. 7). This is in line with a study reporting increased F-actin assembly at the cell periphery in Chinese hamster ovary cells under hyperosmotic stress in order to withstand osmotic shrinkage (Di Ciano et al., 2002). In brain capillary endothelial cells an increased perijunctional F-actin ring that formed in response to hydrocortisone incubation caused a higher cell rigidity and higher TER (Schrot et al., 2005). Indeed it was shown that the perijunctional F-actin ring is not a static structure but undergoes continuous F-actin depolymerization and repolymerization (‘treadmilling’). Although in nascent tight junctions treadmilling is very active, F-actin depolymerization and repolymerization is reduced in mature tight junctions, making them more rigid and stable (Ivanov, 2008).

This is consistent with previous observations that cortisol promoted cellular differentiation and slowed degeneration (Kelly and Wood, 2001a; Kelly and Wood, 2002; Leguen et al., 2007; Wood et al., 2002b). We therefore suspect cortisol to increase the overall stability and rigidity of the epithelial cell layer by promoting its differentiation.

In a previous study we showed that the increased barrier properties of the cortisol-treated epithelium were based on morphological alterations in the mucosal layer of cells such as deeper tight junctions, an increased cell density and smaller, less polygonal cells with increased height and cell–cell contact area (A.M.S., J. Farkas, W. Salvenmoser and B.P., unpublished observation). A stabilizing action of cortisol on paracellular permeability has previously been proposed as a key role of the hormone in reducing passive permeability of the gill epithelium in FW adaptation (Zhou et al., 2003).

In our study cortisol-treated cultures either failed to recover their barrier properties after osmotic stress or at least recovered at a slower rate than respective control cultures (Fig. 11). The general inability of these cultures to regain original barrier tightness was independent of the initial osmotic stress and indicated a decrease in epithelial plasticity. Taken together, the results suggest that cortisol raised tolerance to hyperosmotic salinity by causing stronger and more stabilized perijunctional F-actin (less treadmilling) in highly differentiated epithelia at the cost of decreasing short-term epithelial plasticity.

Cortisol tightens the epithelial cell layer without claudin 28b involvement

Surprisingly, cortisol-treated cultures showed a weak staining for claudin 28b in tight junctions. Hence the higher TER of cortisol-

treated cells was not related to an increase in claudin 28b fluorescence in the tight junction.

Incubation of cell cultures in FW after preincubation with cortisol did not cause a significant reduction of TER or increase of PRD, whereas hyperosmotic saline changed epithelial tightness significantly. However, claudin 28b fluorescence was not significantly different after both treatments (Fig. 7). This demonstrated that in trout pavement cells epithelial tightness was not only related to claudin 28b, but that other factors are involved as well.

Recovery from hypo-osmotic stress (i.e. an increase in osmolarity from 3 to 305 mOsm), however, increased tight junction claudin 28b fluorescence. Thus, the role of cortisol in osmotic adaptation appears to be dependent on the magnitude of the hyperosmotic stress and perhaps on the concentration of osmolytes that the cells have been adapted to originally. Tipsmark et al. also showed in the euryhaline southern flounder (*Paralichthys lethostigma*) that plasma cortisol levels and claudin-4-like protein are both upregulated within the first 24 h when adapting from FW to SW (Tipsmark et al., 2008c). Subsequently, both indicators are downregulated. However, claudin-3-like protein in this study was immediately dowregulated when adapting to SW.

Thus, cortisol affected the distribution of claudin isoforms in tight junctions, although the dynamic response of the claudin 28b content of the tight junctions to osmotic stress was reduced in comparison to that in control conditions. Interestingly, this reduction was accompanied by higher stability of the supporting perijunctional F-actin.

Summary and outlook

The results of our study identify claudin 28b as an important component of trout gill pavement cell tight junctions, contributing to changes in gill epithelium permeability during changes in environmental NaCl concentrations. Changes in osmolarity provoked changes in protein distribution and concentration, whereas changes at the level of mRNA expression were of minor importance. Tight junction remodeling also extended to significant modifications of the perijunctional F-actin ring, which was found to be sensitive to FW and hyperosmotic saline. The separation of the perijunctional F-actin ring from the membrane after hyperosmotic stress may liberate claudin 28b and thus facilitate the dynamic response of the tight junctions. Further studies will demonstrate whether F-actin ring separation and the appearance of pore-like structures at the meeting point of three pavement cells under hyperosmotic conditions are connected to the appearance of apical crypts in saltwater-exposed gills.

Addition of cortisol stabilized the perijunctional F-actin ring. We suspect that this stabilizing action contributed to the reduced osmosensitive behavior of claudin 28b when the hormone was present. In conclusion, our results demonstrate that pavement cells are able to regulate the paracellular pathway *via* dynamic distribution of tight-junction-associated proteins. In this respect the contribution of pavement cell tight junctions to gill permeability may be of pronounced importance.

ACKNOWLEDGEMENTS

We thank Julia Farkas, Reinhard Lackner and Bettina Peer for technical support and Alan Fanning for expert scientific opinion. A.M.S. was supported by the Tyrolean Science Fund (TWF) grant UNI-0404/186.

REFERENCES

Angelow, S., Ahlstrom, R. and Yu, A. S. (2008). Biology of claudins. *Am. J. Physiol. Renal. Physiol.* **295,** F867-F876.

Avella, M. and Ehrenfeld, J. (1997). Fish gill respiratory cells in culture: a new model for Cl(–)-secreting epithelia. *J. Membrane Biol.* **156**, 87-97.

Azenha, M. A., Evangelista, R., Martel, F. and Vasconcelos, M. T. (2004). Estimation of the human intestinal permeability of butyltin species using the Caco-2 cell line model. *Food Chem. Toxicol.* **42**, 1431-1442.

Bagherie-Lachidan, M., Wright, S. I. and Kelly, S. P. (2008). Claudin-3 tight junction proteins in *Tetraodon nigroviridis*: cloning, tissue-specific expression, and a role in hydromineral balance. *Am. J. Physiol. Regul. Integr. Comp. Physiol.* **294**, R1638-R1647.

Bagherie-Lachidan, M., Wright, S. I. and Kelly, S. P. (2009). Claudin-8 and -27 tight junction proteins in puffer fish *Tetraodon nigroviridis* acclimated to freshwater and seawater. *J. Comp. Physiol. B* **179**, 419-431.

Bassam, B. J., Caetano-Anolles, G. and Gresshoff, P. M. (1991). Fast and sensitive silver staining of DNA in polyacrylamide gels. *Anal. Biochem.* **196**, 80.

Boutet, I., Long Ky, C. L. and Bonhomme, F. (2006). A transcriptomic approach of salinity response in the euryhaline teleost, *Dicentrarchus labrax*. *Gene* **379**, 40-50.

Bui, P., Bagherie-Lachidan, M. and Kelly, S. P. (2010). Cortisol differentially alters claudin isoforms in cultured puffer fish gill epithelia. *Mol. Cell Endocrinol.* **317**, 120-126.

Burg, M. B., Ferraris, J. D. and Dmitrieva, N. I. (2007). Cellular response to hyperosmotic stresses. *Physiol. Rev.* **87**, 1441-1474.

Chasiotis, H., Wood, C. M. and Kelly, S. P. (2010). Cortisol reduces paracellular permeability and increases occludin abundance in cultured trout gill epithelia. *Mol. Cell Endocrinol.* **323**, 232-238.

Colegio, O. R., Van Itallie, C., Rahner, C. and Anderson, J. M. (2003). Claudin extracellular domains determine paracellular charge selectivity and resistance but not tight junction fibril architecture. *Am. J. Physiol. Cell. Physiol.* **284**, C1346-C1354.

Daborn, K., Cozzi, R. R. and Marshall, W. S. (2001). Dynamics of pavement cell-chloride cell interactions during abrupt salinity change in *Fundulus heteroclitus*. *J. Exp. Biol.* **204**, 1889-1899.

Di Ciano, C., Nie, Z., Szaszi, K., Lewis, A., Uruno, T., Zhan, X., Rotstein, O. D., Mak, A. and Kapus, A. (2002). Osmotic stress-induced remodeling of the cortical cytoskeleton. *Am. J. Physiol. Cell. Physiol.* **283**, C850-C865.

Dorovini-Zis, K., Bowman, P. D., Betz, A. L. and Goldstein, G. W. (1987). Hyperosmotic urea reversibly opens the tight junctions between brain capillary endothelial cells in cell culture. *J. Neuropathol. Exp. Neurol.* **46**, 130-140.

Ernst, S. A., Dodson, W. C. and Karnaky, K. J., Jr (1980). Structural diversity of occluding junctions in the low-resistance chloride-secreting opercular epithelium of seawater-adapted killifish (*Fundulus heteroclitus*). *J. Cell Biol.* **87**, 488-497.

Evans, D. H., Piermarini, P. M. and Choe, K. P. (2005). The multifunctional fish gill: dominant site of gas exchange, osmoregulation, acid-base regulation, and excretion of nitrogenous waste. *Physiol. Rev.* **85**, 97-177.

Fanning, A. S. (2001). Organization and regulation of the tight junction by the actin-myosin cytoskeleton. In *Tight Junctions*, second edition (ed. M. Cereijido and J. M. Anderson), pp. 265-284. Boca Raton, FL: CRC Press.

Gilmour, K. M., Pärt, P., Prunet, P., Pisam, M., McDonald, D. G. and Wood, C. M. (1998). Permeability and morphology of a cultured branchial epithelium from the rainbow trout during prolonged apical exposure to fresh water. *J. Exp. Zool.* **281**, 531-545.

Hoffmann, R., Krallinger, M., Andres, E., Tamames, J., Blaschke, C. and Valencia, A. (2005). Text mining for metabolic pathways, signaling cascades, and protein networks. *Sci. STKE* **2005**, e21.

Hwang, P. P. (1987). Tolerance and ultrastructural responses of branchial chloride cells to salinity changes in the euryhaline teleost *Oreochromis mossambicus*. *Mar. Biol.* **94**, 643-649.

Ivanov, A. I. (2008). Actin motors that drive formation and disassembly of epithelial apical junctions. *Front. Biosci.* **13**, 6662-6681.

Jovov, B., Wills, N. K. and Lewis, S. A. (1991). A spectroscopic method for assessing confluence of epithelial cell cultures. *Am. J. Physiol.* **261**, C1196-C1203.

Kalujnaia, S., McWilliam, I. S., Zaguinaiko, V. A., Feilen, A. L., Nicholson, J., Hazon, N., Cutler, C. P. and Cramb, G. (2007). Transcriptomic approach to the study of osmoregulation in the European eel *Anguilla anguilla*. *Physiol. Genomics* **31**, 385-401.

Karnaky, K. J., Jr (1992). Teleost osmoregulation: changes in the tight junction in response to the salinity of the environment. In *Tight Junctions*, second edition (ed. M. Cereijido and J. M. Anderson), pp. 265-284. Boca Raton, FL: CRC Press.

Kelly, S. P. and Wood, C. M. (2001a). Effect of cortisol on the physiology of cultured pavement cell epithelia from freshwater trout gills. *Am. J. Physiol. Regul. Integr. Comp. Physiol.* **281**, R811-R820.

Kelly, S. P. and Wood, C. M. (2001b). The physiological effects of 3,5′,3′-triiodo-L-thyronine alone or combined with cortisol on cultured pavement cell epithelia from freshwater rainbow trout gills. *Gen. Comp. Endocrinol.* **123**, 280-294.

Kelly, S. P. and Wood, C. M. (2002). Cultured gill epithelia from freshwater tilapia (*Oreochromis niloticus*): effect of cortisol and homologous serum supplements from stressed and unstressed fish. *J. Membr. Biol.* **190**, 29-42.

Kim, J. H., Yu, Y. S., Kim, J. H., Kim, K. W. and Min, B. H. (2007). The role of clusterin in in vitro ischemia of human retinal endothelial cells. *Curr. Eye Res.* **32**, 693-698.

Leguen, I., Cauty, C., Odjo, N., Corlu, A. and Prunet, P. (2007). Trout gill cells in primary culture on solid and permeable supports. *Comp. Biochem. Physiol. A* **148**, 903-912.

Lewis, S. A. (2002). Assessing epithelial cell confluence by spectroscopy. In *Epithelial Cell Culture Protocols* (ed. C. Wise), pp. 329-336. Totowa, New Jersey: Humana Press.

Liang, P., Zhu, W., Zhang, X., Guo, Z., O'Connell, R. P., Averboukh, L., Wang, F. and Pardee, A. B. (1994). Differential display using one-base anchored oligo-dT primers. *Nucleic Acids Res.* **22**, 5763-5764.

Loh, Y. H., Christoffels, A., Brenner, S., Hunziker, W. and Venkatesh, B. (2004). Extensive expansion of the claudin gene family in the teleost fish, *Fugu rubripes*. *Genome Res.* **14**, 1248-1257.

Marshall, W. S. (1995). Transport processes in isolated teleost epithelia: opercular epithelium and urinary bladder. In *Fish Physiology*, Vol. 14 (ed. C. M. Wood and T. J. Shuttleworth), pp. 1-23. Academic Press.
Matter, K. and Balda, M. S. (2003). Functional analysis of tight junctions. *Methods* **30**, 228-234.
Michaud, J.-L. R., Chaisson, K. M., Parks, R. J. and Kennedy, C. R. J. (2006). FSGS-associated α-actinin-4 (K256E) impairs cytoskeletal dynamics in podocytes. *Kidney Int.* **70**, 1054-1061.
Mistry, A. C., Kato, A., Tran, Y. H., Honda, S., Tsukada, T., Takei, Y. and Hirose, S. (2004). FHL5, a novel actin fiber-binding protein, is highly expressed in gill pillar cells and responds to wall tension in eels. *Am. J. Physiol. Regul. Integr. Comp. Physiol.* **287**, R1141-R1154.
Nilsson, H., Dragomir, A., Ahlander, A., Johannesson, M. and Roomans, G. M. (2007). Effects of hyperosmotic stress on cultured airway epithelial cells. *Cell Tissue Res.* **330**, 257-269.
Pan, F., Zarate, J. and Bradley, T. M. (2002). A homolog of the E3 ubiquitin ligase Rbx1 is induced during hyperosmotic stress of salmon. *Am. J. Physiol. Regul. Integr. Comp. Physiol.* **282**, R1643-R1653.
Pan, F., Zarate, J., Choudhury, A., Rupprecht, R. and Bradley, T. M. (2004). Osmotic stress of salmon stimulates upregulation of a cold inducible RNA binding protein (CIRP) similar to that of mammals and amphibians. *Biochimie* **86**, 451-461.
Patrie, K. M., Drescher, A. J., Welihinda, A., Mundel, P. and Margolis, B. (2002). Interaction of two actin-binding proteins, synaptopodin and actinin-4, with the tight junction protein MAGI-1. *J. Biol. Chem.* **277**, 30183-30190.
Paye, J. M., Akers, R. M., Huckle, W. R. and Forsten-Williams, K. (2007). Autocrine production of insulin-like growth factor-I (IGF-I) affects paracellular transport across epithelial cells in vitro. *Cell Commun. Adhes.* **14**, 85-98.
Peixoto, E. B. and Collares-Buzato, C. B. (2005). Protamine-induced epithelial barrier disruption involves rearrangement of cytoskeleton and decreased tight junction-associated protein expression in cultured MDCK strains. *Cell Struct. Funct.* **29**, 165-178.
Rasmussen, M., Alexander, R. T., Darborg, B. V., Mobjerg, N., Hoffmann, E. K., Kapus, A. and Pedersen, S. F. (2008). Osmotic cell shrinkage activates ezrin/radixin/moesin (ERM) proteins: activation mechanisms and physiological implications. *Am. J. Physiol. Cell. Physiol.* **294**, C197-C212.
Rathore, R., Jain, J. P., Srivastava, A., Jachak, S. M. and Kumar, N. (2008). Simultaneous determination of hydrazinocurcumin and phenol red in samples from rat intestinal permeability studies: HPLC method development and validation. *J. Pharm. Biomed. Anal.* **46**, 374-380.
Sakamoto, T., Ojima, N. and Yamashita, M. (2000). Induction of mRNAs in response to acclimation of trout cells to different osmolalities. *Fish Physiol. Biochem.* **22**, 255-262.
Sardet, C., Pisam, M. and Maetz, J. (1979). The surface epithelium of teleostean fish gills. Cellular and junctional adaptations of the chloride cell in relation to salt adaptation. *J. Cell Biol.* **80**, 96-117.
Schrot, S., Weidenfeller, C., Schaffer, T. E., Robenek, H. and Galla, H. J. (2005). Influence of hydrocortisone on the mechanical properties of the cerebral endothelium in vitro. *Biophys. J.* **89**, 3904-3910.
Shen, L. and Turner, J. R. (2005). Actin depolymerization disrupts tight junctions via caveolae-mediated endocytosis. *Mol. Biol. Cell* **16**, 3919-3936.
Shen, L., Black, E. D., Witkowski, E. D., Lencer, W. I., Guerriero, V., Schneeberger, E. E. and Turner, J. R. (2006a). Myosin light chain phosphorylation regulates barrier function by remodeling tight junction structure. *J. Cell. Sci.* **119**, 2095-2106.
Shen, Y., Jia, Z., Nagele, R. G., Ichikawa, H. and Goldberg, G. S. (2006b). Src uses Cas to suppress Fhl1 in order to promote nonanchored growth and migration of tumor cells. *Cancer Res.* **66**, 1543-1552.
Sonoda, N., Furuse, M., Sasaki, H., Yonemura, S., Katahira, J., Horiguchi, Y. and Tsukita, S. (1999). Clostridium perfringens enterotoxin fragment removes specific claudins from tight junction strands: evidence for direct involvement of claudins in tight junction barrier. *J. Cell Biol.* **147**, 195-204.
Suzuki, Y., Itakura, M., Kashiwagi, M., Nakamura, N., Matsuki, T., Sakuta, H., Naito, N., Takano, K., Fujita, T. and Hirose, S. (1999). Identification by differential display of a hypertonicity-inducible inward rectifier potassium channel highly expressed in chloride cells. *J. Biol. Chem.* **274**, 11376-11382.
Takei, Y. and Hirose, S. (2002). The natriuretic peptide system in eels: a key endocrine system for euryhalinity? *Am. J. Physiol. Regul. Integr. Comp. Physiol.* **282**, R940-R951.
Tipsmark, C. K., Baltzegar, D. A., Ozden, O., Grubb, B. J. and Borski, R. J. (2008a). Salinity regulates claudin mRNA and protein expression in the teleost gill. *Am. J. Physiol. Regul. Integr. Comp. Physiol.* **294**, R1004-R1014.
Tipsmark, C. K., Kiilerich, P., Nilsen, T. O., Ebbesson, L. O., Stefansson, S. O. and Madsen, S. S. (2008b). Branchial expression patterns of claudin isoforms in Atlantic salmon during seawater acclimation and smoltification. *Am. J. Physiol. Regul. Integr. Comp. Physiol.* **294**, R1563-R1574.
Tipsmark, C. K., Luckenbach, J. A., Madsen, S. S., Kiilerich, P. and Borski, R. J. (2008c). Osmoregulation and expression of ion transport proteins and putative claudins in the gill of southern flounder (*Paralichthys lethostigma*). *Comp. Biochem. Physiol.* **150A**, 265-273.
Tipsmark, C. K., Jorgensen, C., Brande-Lavridsen, N., Engelund, M., Olesen, J. H. and Madsen, S. S. (2009). Effects of cortisol, growth hormone and prolactin on gill claudin expression in Atlantic salmon. *Gen. Comp. Endocrinol.* **163**, 270-277.
Tsai, J. C. and Hwang, P. P. (1998). Effects of wheat germ agglutinin and colchicine on microtubules of the mitochondria-rich cells and Ca^{2+} uptake in tilapia (*Oreochromis mossambicus*) larvae. *J. Exp. Biol.* **201**, 2263-2271.
Tsukita, S., Furuse, M. and Itoh, M. (2001). Multifunctional strands in tight junctions. *Nat. Rev. Mol. Cell. Biol.* **2**, 285-293.
Van Itallie, C., Rahner, C. and Anderson, J. M. (2001). Regulated expression of claudin-4 decreases paracellular conductance through a selective decrease in sodium permeability. *J. Clin. Invest.* **107**, 1319-1327.
Varma, M. V., Kapoor, N., Sarkar, M. and Panchagnula, R. (2004). Simultaneous determination of digoxin and permeability markers in rat in situ intestinal perfusion samples by RP-HPLC. *J. Chromatogr. B Analyt. Technol. Biomed. Life Sci.* **813**, 347-352.
Warskulat, U., Kreuels, S., Muller, H. W. and Haussinger, D. (2001). Identification of osmosensitive and ammonia-regulated genes in rat astrocytes by Northern blotting and differential display reverse transcriptase-polymerase chain reaction. *J. Hepatol.* **35**, 358-366.
Wiggins, A. K., Shen, P. J. and Gundlach, A. L. (2003). Delayed, but prolonged increases in astrocytic clusterin (ApoJ) mRNA expression following acute cortical spreading depression in the rat: evidence for a role of clusterin in ischemic tolerance. *Brain Res. Mol. Brain Res.* **114**, 20-30.
Wilson, J. M., Laurent, P., Tufts, B. L., Benos, D. J., Donowitz, M., Vogl, A. W. and Randall, D. J. (2000). NaCl uptake by the branchial epithelium in freshwater teleost fish: an immunological approach to ion-transport protein localization. *J. Exp. Biol.* **203 Pt 15**, 2279-2296.
Wood, C. M. and Pärt, P. (1997). Cultured branchial epithelia from freshwater fish gills. *J. Exp. Biol.* **200**, 1047-1059.
Wood, C. M., Gilmour, K. M. and Pärt, P. (1998). Passive and active transport properties of a gill model, the cultured branchial epithelium of the freshwater rainbow trout (*Oncorhynchus mykiss*). *Comp. Biochem. Physiol.* **119A**, 87-96.
Wood, C. M., Eletti, B. and Pärt, P. (2002a). New methods for the primary culture of gill epithelia from freshwater rainbow trout. *Fish Physiol. Biochem.* **26**, 329-344.
Wood, C. M., Kelly, S. P., Zhou, B., Fletcher, M., O'Donnell, M., Eletti, B. and Pärt, P. (2002b). Cultured gill epithelia as models for the freshwater fish gill. *Biochim. Biophys. Acta* **1566**, 72-83.
Zhou, B., Kelly, S. P., Ianowski, J. P. and Wood, C. M. (2003). Effects of cortisol and prolactin on Na^+ and Cl^- transport in cultured branchial epithelia from FW rainbow trout. *Am. J. Physiol. Regul. Integr. Comp. Physiol.* **285**, R1305-R1316.
Zhou, B., Liu, W., Wu, R. S. and Lam, P. K. (2005). Cultured gill epithelial cells from tilapia (*Oreochromis niloticus*): a new in vitro assay for toxicants. *Aquat. Toxicol.* **71**, 61-72.